Spring 2015

# Genetic Relations of West Spanish Peak Stock, South-Central Colorado, with Surrounding Radial Dikes Containing Cognate Xenoliths and Miarolitic Cavities

Stewart Ray
Stewart.Ray@Colorado.EDU

# Genetic Relations of West Spanish Peak Stock, South-Central Colorado, with Surrounding Radial Dikes Containing Cognate Xenoliths and Miarolitic Cavities

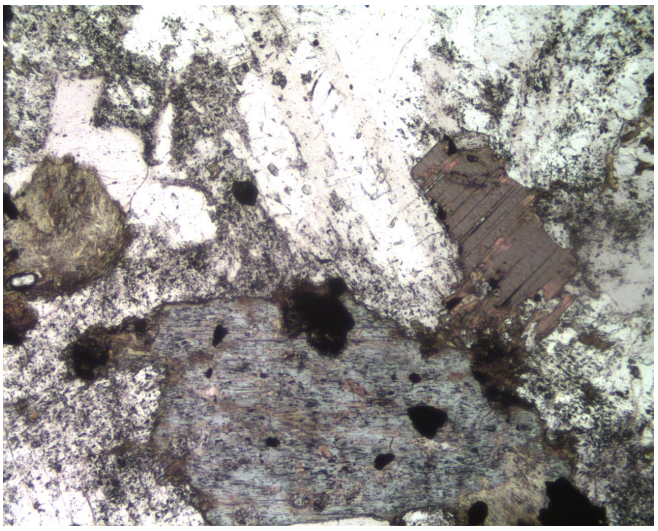

West Spanish Peak Stock

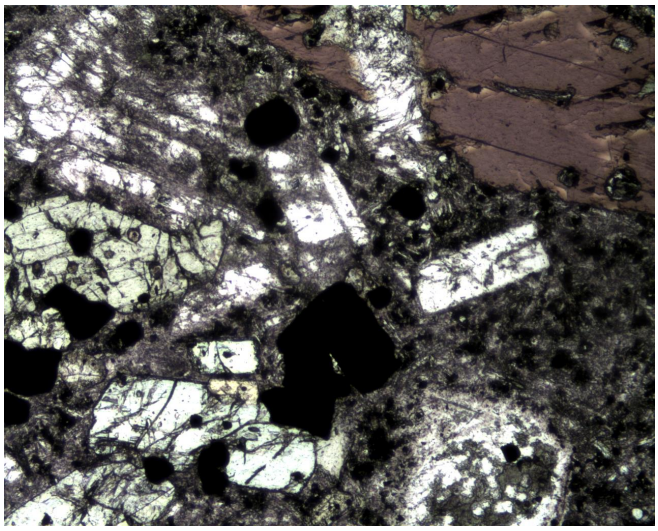

Radial Dike

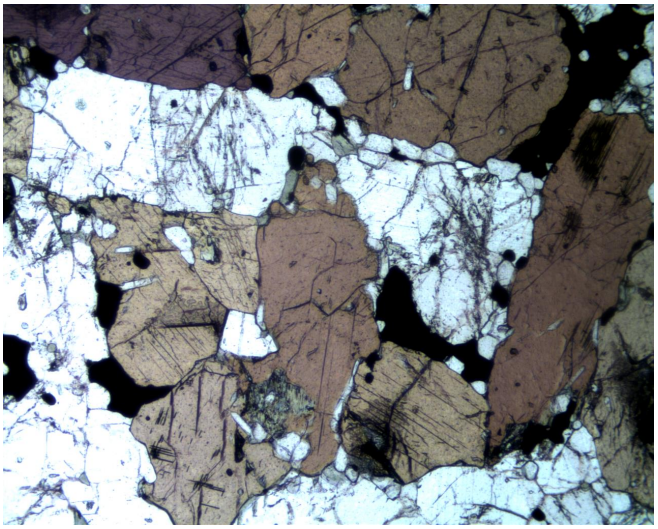

Cognate Xenolith

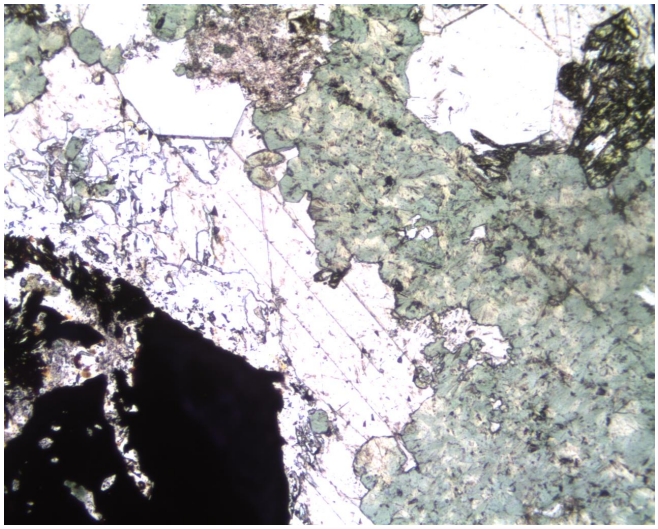

Miarolitic Cavity

Undergraduate Thesis for Departmental Honors from the University of Colorado, Boulder

Department of Geological Sciences

Stewart M. Ray

Defense Date: April 7$^{h}$, 2015

Thesis Defense Committee:

Thesis Advisor: Charles Stern – Department of Geological Sciences

Committee Member: Lang Farmer – Department of Geological Sciences

Commmittee Memeber: Faan Tone Liu – Department of Mathematics

# Genetic Relations of West Spanish Peak Stock, South-Central Colorado, with Surrounding Radial Dikes Containing Cognate Xenoliths and Miarolitic Cavities

Stewart M. Ray
Department of Geological Sciences

## Abstract

The Spanish Peaks intrusive suite in south-central Colorado includes various mid-Tertiary intrusions, which includes the plutonic stocks of the Spanish Peaks themselves, as well as various dikes, sills, and volcanic plugs. This study specifically focuses on the relationship between the plutonic stock of the West Spanish Peak and a group of radial dikes centered on this mountain. The goal of this thesis is to determine if the radial dike swarm and the West Spanish Peak stock potentially share a common magma source based on their temporal, geochemical, and isotopic relationships.

The West Spanish peak is a holocrystaline quartz monzanite plutonic stock, and its surrounding hypocystalline radial dikes range from mafic to felsic in composition. Contained within the radial dikes surrounding the peak are cognate xenoliths and miarolitic cavities, features which have not been described in this geologic setting before. The holocrystalline cognate xenoliths in the radial dikes have gabbroic compositions. The miarolitic cavities are composed of a variety of both mafic and felsic minerals in concentric rims towards the center of the cavities. From the petrographic, major and minor oxide, trace element, and $^{87}Sr/^{86}Sr$ isotopic analyses I conducted on these samples two major conclusions have been drawn. First, the West Spanish Peak stock, its surrounding radial dikes, and the cognate xenoliths included into the radial dikes are likely to be co-genetic, most probably forming from a single parent-magma body. Secondly, the miarolitic cavities in the radial dikes formed during a paleo-groundwater event, or series of events, which occurred after the emplacement of the radial dike swarm, but probably soon after when the local groundwaters were still heated.

**Table of Contents**


Chapter 1 – Introduction *Page*

General....1

Geologic Setting....3

Methods....7

Chapter 2 – Petrology

Introduction....14

West Spanish Peak Stock....14

Radial Dikes....16

Cognate Xenoliths....21

Miarolitic Cavities....24

Chapter 3 – Mineral Chemistry

Introduction....27

Clinopyroxene....27

Amphiboles....31

Feldspars....35

Biotite....37

Oxides....39

Sulfides....46

Chapter 4 – Bulk Rock Major and Minor Oxide, Trace Element, and Isotopic Chemistry

Introduction....50

Major and Minor Oxides....50

Trace and Rare-Earth Elements (REEs)....53

Isotopic Data....58

Chapter 5 – Discussion and Conclusions

Introduction....59

Isotopic $^{87}Sr/^{86}Sr$ Implications for the Spanish Peaks Region....60

Cogenetic Model for West Spanish Peak, Radial Dikes, and Cognate Xenoliths....63

Future Work....67

Acknowledgments.....67
References.....68

# Chapter 1

## *Introduction*

### General:

The Spanish Peaks, located in south-central Colorado (Fig. 1.1) are two prominent mountains which serve as distinct landmarks that can be seen for many miles to the north and east when approaching the Rocky Mountains from the Great Plains. The peaks tower above Great Plains to the east, sitting on their western edge (Fig. 1.2). These peaks almost match the heights of mountains along the continental divide in the Sangre de Cristo Mountains just to the west. The Spanish Peaks lie in a drainage basin called the Raton Basin which spans an area from Raton in northern New Mexico (Fig. 1.3 and 1.4), northward along the eastern front of the Sangre de Cristo mountains past Walsenburg, Colorado and extending into the valley between the Sangre de Cristo Mountains and the Wet Mountains (Fig. 1.5).

The Spanish Peaks themselves are two large plutonic stocks that are located East of the Sangre De Cristo mountains, west of Interstate-25, north of the community of Stonewall, and just south of the town of La Veta, Colorado. West Spanish Peak and East Spanish Peak intruded between 25 to 21 Ma (millions of years ago) (Fig. 1.3 and Fig. 1.8; Miggins (2002) and Penn and Lindsey (2009)), about the same time as the beginning of the opening of the Rio Grnade Rift. They are of slightly different composition indicating that they represent two separate intrusive events.

Along with the stocks that compose Spanish Peaks, there are many other intrusive features in the surrounding area of the Raton Basin, including dikes, sills, and even volcanic plugs that also were fed by magmas associated with the opening of the Rio Grande rift. In fact there are different groupings of dikes that cross one another throughout the Raton basin and stand on the scale of meters to tens of meters above the surface because they are more resistant to weathering than the surrounding sediments. The dikes have been characterized and classified in previous extensive field studies of this area, notably by Penn (1994), Miggins (2002), and Penn and Lindsey (2009), who both strove to determine the geochemical and geochronological relationships of a diverse suite of rocks in the Spanish Peaks area.

The radial dike system surrounding West Spanish Peak is the primary focus of this study. Within the radial dikes there have been both cognate xenoliths as well as miarolitic cavities that have been respectively identified and described by Contreras (2014) and Johnson (2014). The purpose of this study is to investigate in greater detail the geochemical characteristics of these included features within the radial dikes to determine if the radial dikes and the West Spanish Peak pluton potentially share a

common magma source. What I did in this study was to collect samples of radial dikes containing gabbroic xenoliths and miarolitic cavities, prepare thin sections of these samples and describe them petrologically, determine their mineral chemistry with the electron microprobe , powder them for major and trace-element chemical analysis, and obtain Sr-isotopic data from a selection of these samples.

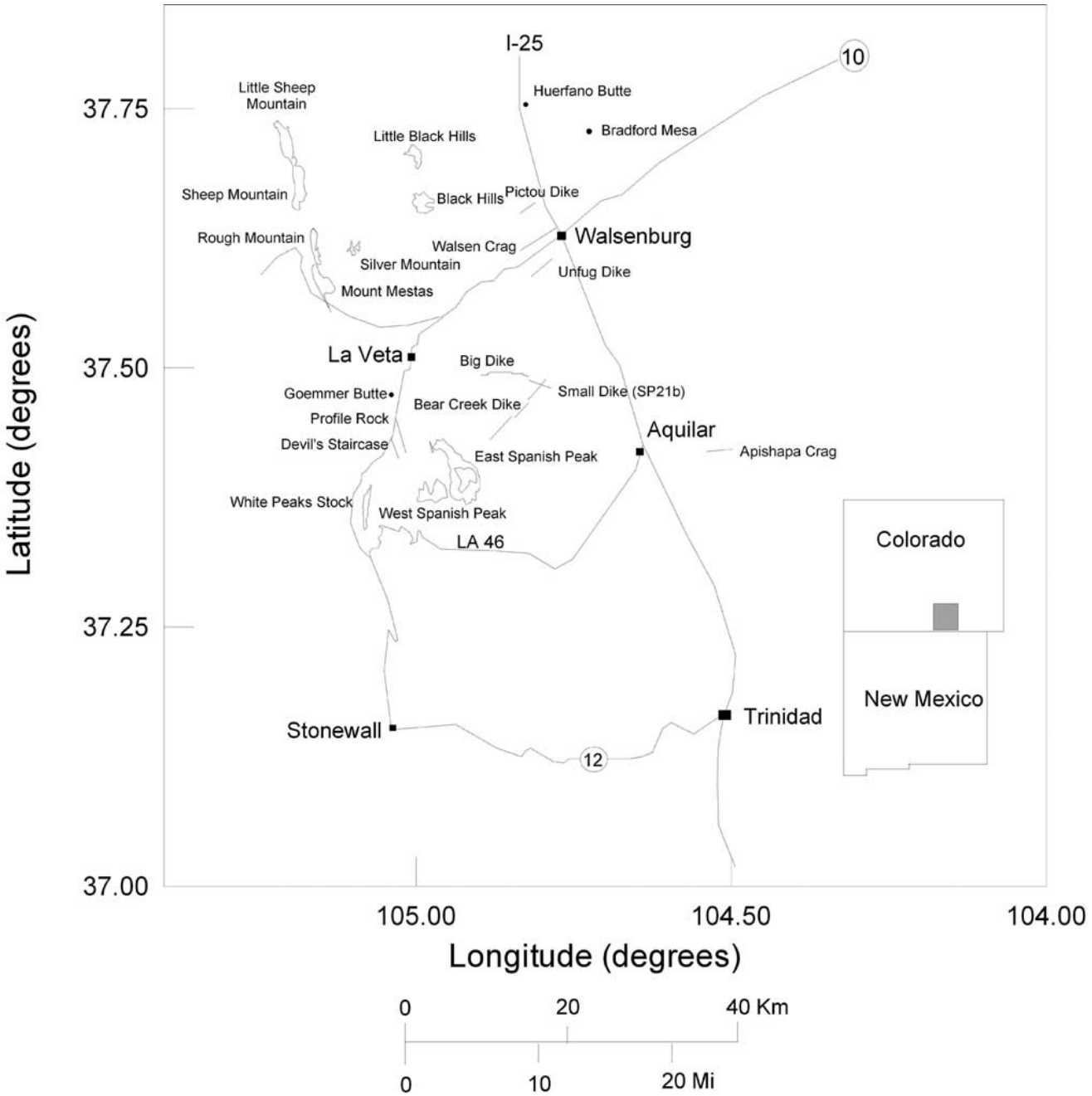


**Figure 1.1:** A simplified map from Penn and Lindsey (2009) of the roads and major intrusive features within the Raton Basin in south-central Colorado. The Spanish Peaks appear near the center of the image in between the towns of La Veta, Aquilar and Stonewall, Colorado.

**Geological Setting:**

The Spanish Peaks occur on the eastern flank of the Laramide Deformation front, but based on their ages the timing of their formation is associated with the opening of the Rio Grande rift. The rifting, which began about 25 million years ago, during the mid-Tertiary thinned the crust as upwelling mantle rose towards the surface, causing the formation of the San Luis valley just west of the Sangre de Cristo Mountains, and supplying magmas that fed to the surface along weak points created in the crust. These weak points in the crust were old faults associated with the rising of the Sangre de Cristo mountains during the Laramide orogeny. It is these magmas that are the source of material that generated the plutonic stocks that are now known as the Spanish Peaks, as well as the magma source for the dikes surrounding the stocks.

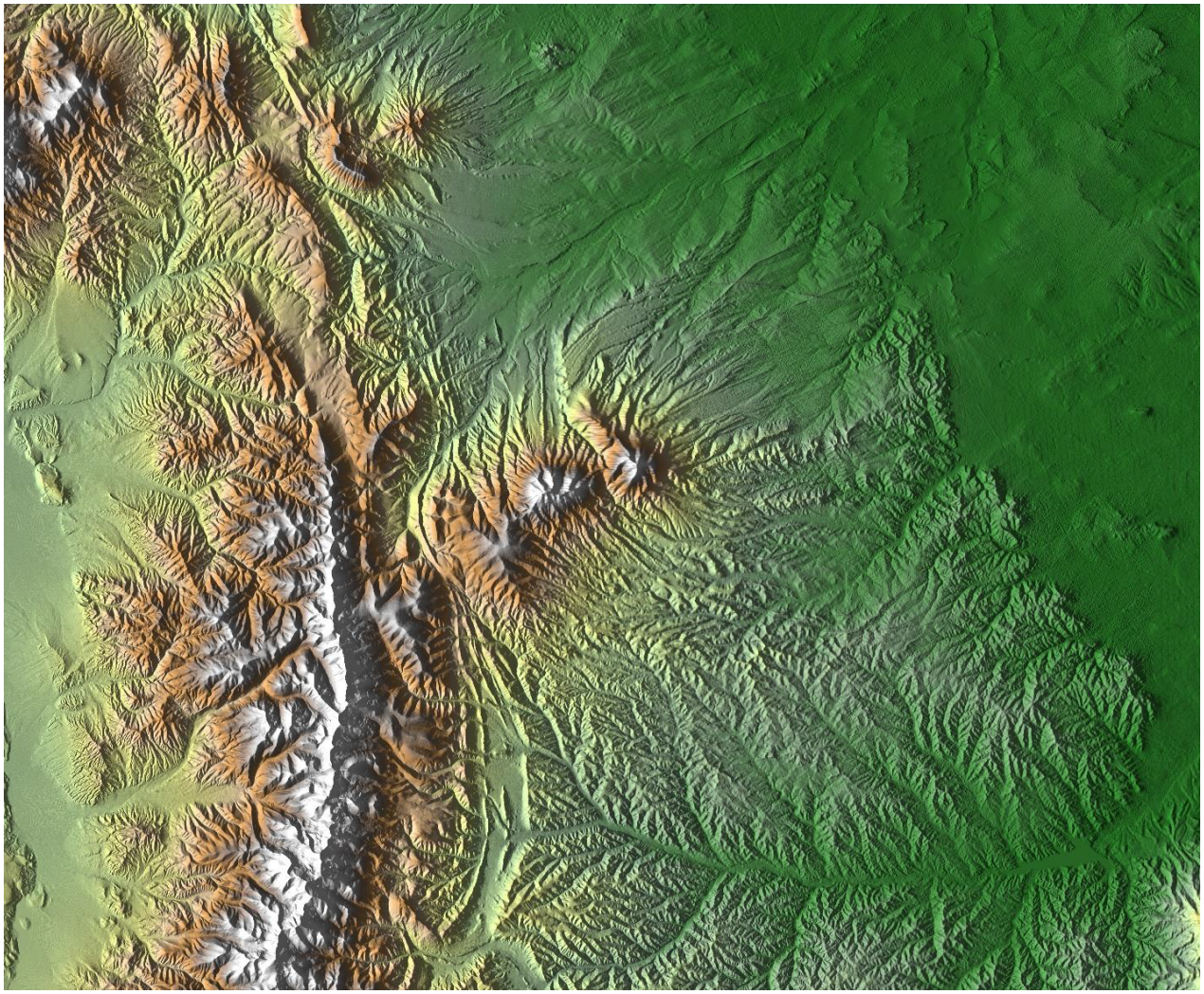

**Figure 1.2:** Digital Elevation Model (DEM) of the Spanish Peaks region. Spanish Peaks are the topographically high points near the center of the image east of the Sangre de Cristo mountains.

The intrusion of the Spanish Peaks is associated with the opening of the Rio Grande rift, which began approximately 25 million years ago. The Rio Grande Rift is a large continental rift system in the Western North America that extends from central Mexico northward up through central New Mexico and into South-central Colorado. The opening of rift systems is associated with the upwelling of mantle asthenosphere which is either caused by the decompression of of overlying material, or by the addition of heat and/or volatiles to the mantle material. In the context of the Rio Grande rift, a continental rift system, the upwelling mantle asthenosphere induces a large portion or partial melting within the overlying crust. The result of this interaction between the rising mantle and the crust not only induces brittle deformation by prying the crust apart to accommodate for the upwelling mantle at the surface, but also ductile deformation in the form of partial melting and the subsequent emplacement of rising melts into the overlying crust. These melts rose into magma chambers in the crust, two of which cooled slowly over a long period of time to form the individual Spanish Peaks. Since their crystallization erosion has stripped away overlying sediments to leave behind the intrusive crystalline rock, which is more resistant to weathering, towering above their surroundings.

The Spanish Peaks are surrounded by three distinct groups of dikes. The first group of dikes runs sub-parallel to one another, striking roughly N80E. The second group of dikes is a radial group of dikes centered on West Spanish Peak, and is the main group of dikes that will be incorporated into this study. The final group of dikes are miscellaneous dikes that seem to be neither related to the sub-parallel set or the radial group of dikes. The samples collected in this study were from radial dikes focused on West Spanish Peak, found relatively close to the igneous stock on its southwestern flank. While there is published results that say these radial dikes do not contact West Spanish Peak, Johnson (1961, 1968), it appears that the radial dikes here, along with other very large, regionally extensive radial dikes observed in the field during sample collection (Fig. 1.6), are heading straight into the igneous stock. There is not an observable contact, the limbs of the dike appear to diffuse into sedimentary layers adorning the mountain that were thermally heated by the plutonic body of West Spanish Peak, and are still preserved around the highest exposed level of the peaks (Fig. 1.6). This observation is relevant because it is an indication that the radial dikes and the igneous stock contact one another, spatially indicating that these features potentially share a common magma source.

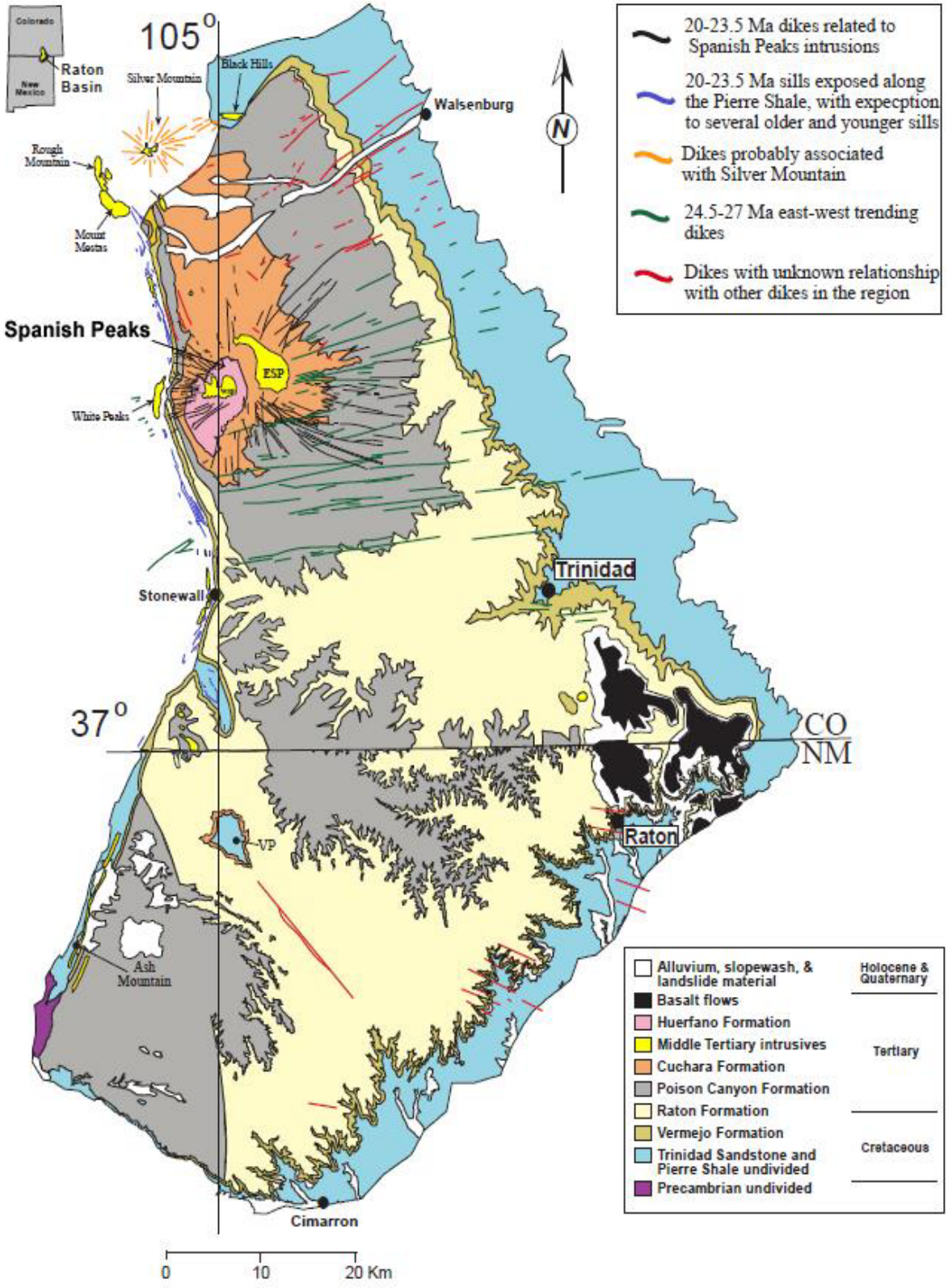


**Figure 1.3:** Geological Map of the Raton Basin showing grouping and intrusion age date ranges of radial dikes (Miggins, 2002).

**West** **East**

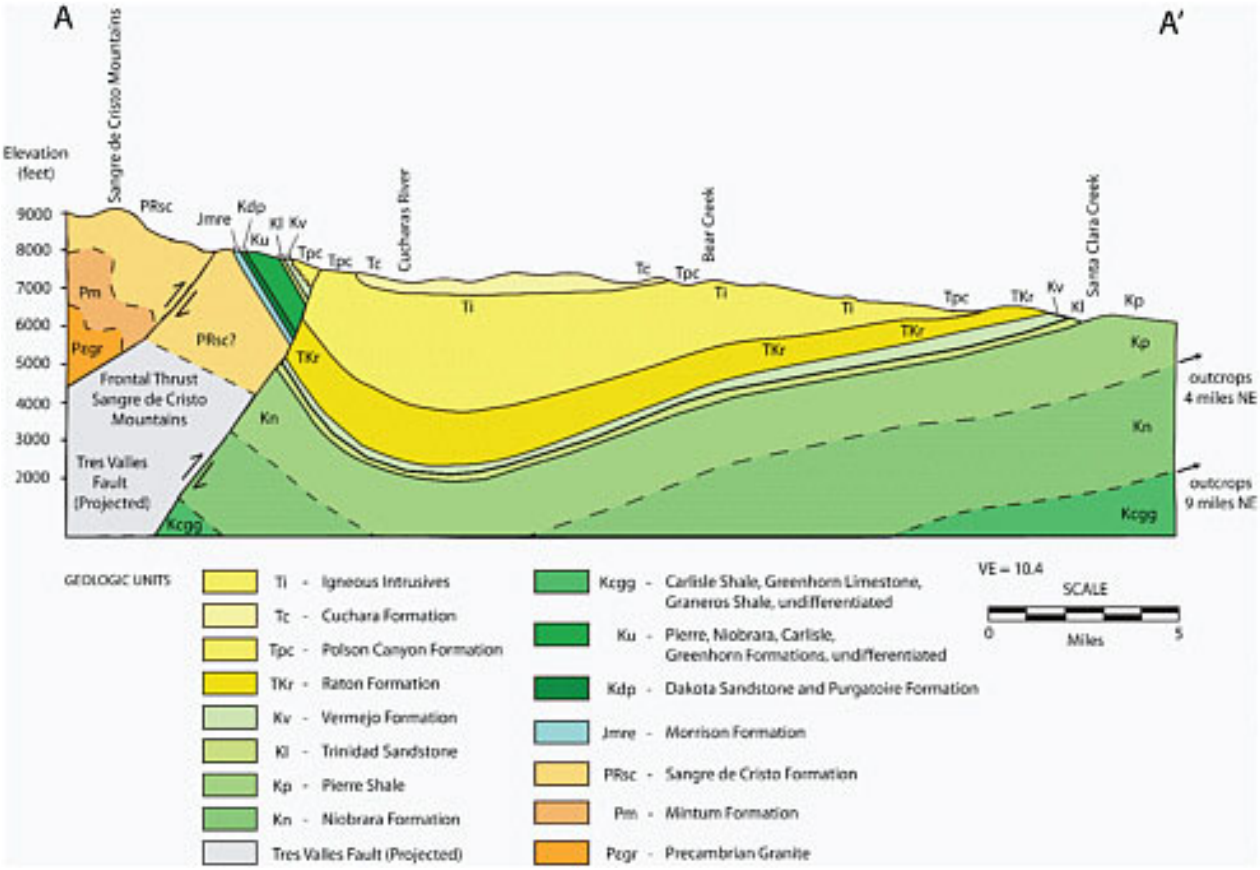


**Figure 1.4:** Geological cross-section of the Raton Basin. Spanish Peaks are located on the western end of the cross section but on the eastern edge of the Sangre de Cristo Mountains (near the area of thrust faulting).

West Spanish Peak and its surrounding radial dikes are a part of the 30 square mile Spanish Peaks intrusive suite which is located in south-central Colorado. The Spanish Peaks are twin conical peaks that are located on the eastern edge of the Sangre de Cristo mountains, approximately 30 kilometers southwest of the town of Walsenburg, Colorado. The East Spanish Peak and West Spanish peak are ~12,700 feet and ~13,600 feet above sea level respectively, and together loom approximately 7,500 feet above the sedimentary cover composing the Great Plains to the east. The Spanish peaks intrude into Paleozoic sediments that compose the La-Veta syncline and the Raton Basin near the major thrust faults associated with the Sangre de Cristo mountains. The rising asthenosphere associated with the Rio Grande Rift was occurring just to West of the Sangre de Cristo mountains, below the San Luis Valley. This rising asthenoshpere caused decompression melting of the mantle, ultimately leading to the origin of magmas which climbed up the margin of the Rio Grande rift. Magmas crept up these faults into their final emplacement in the upper crust as the plutonic stocks now known as the Spanish

Peaks.

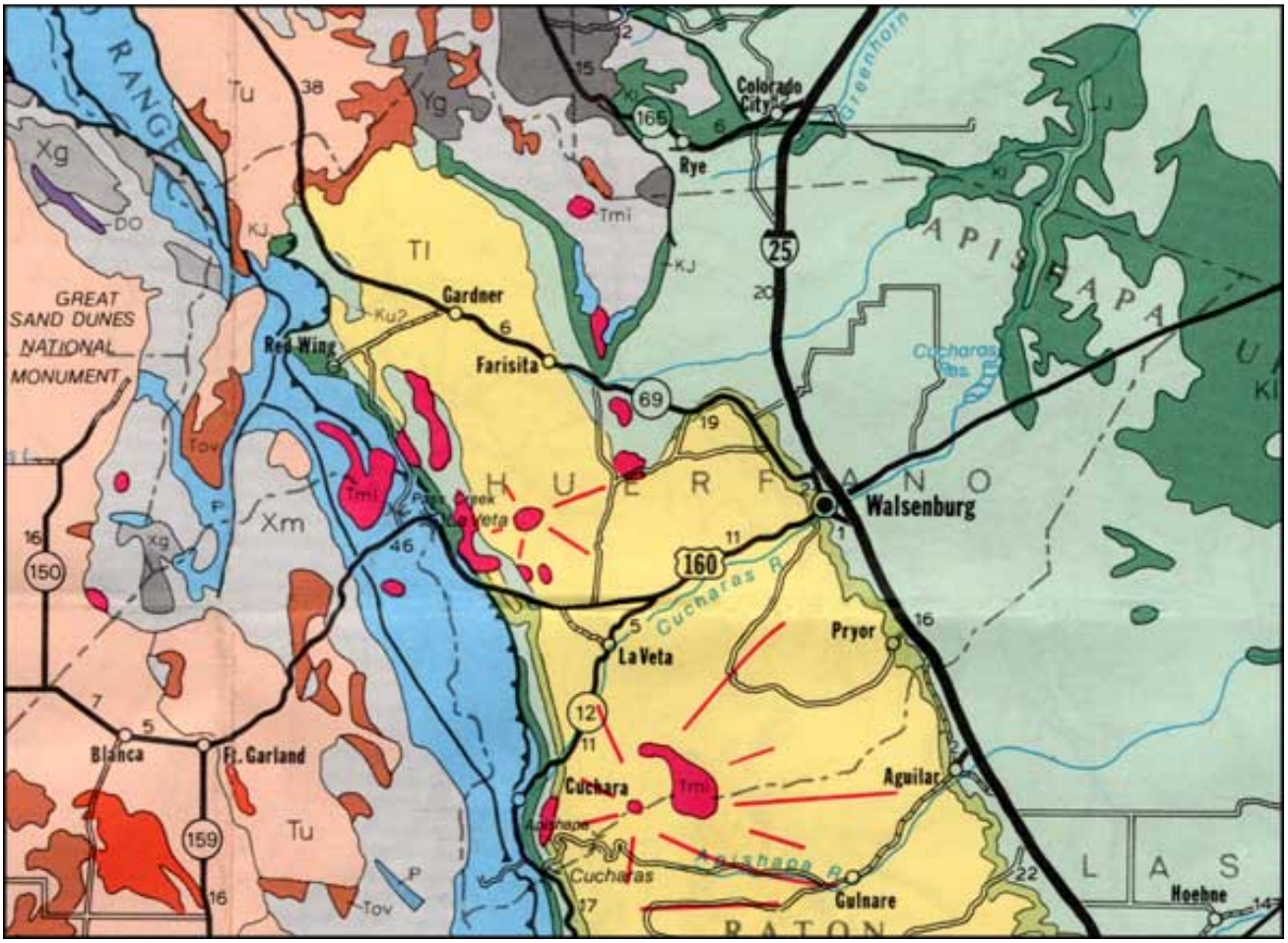


**Figure 1.5:** Location of Spanish Peaks on a simplified geological map of Huerfano County, Colorado and the surrounding area. The Spanish Peaks and other mid-Tertiary plutons are portrayed as bright red patches in the central-bottom portion of the map; south of U.S. highway 160 and west of Interstate-25. A few prominent dikes surrounding the peaks are also portrayed on this map as the bright red lines protruding from the Spanish Peaks. The sedimentary rocks of the Raton basin are indicated as the yellow geologic unit here.

**Methods:**

Samples for this study were collected from the southwestern flank of West Spanish Peak (Fig. 1.6), and were used in comparison to samples collected by Contreras (2014) and Johnson (2014) from the same area. The variety of samples included into this study aims to put the congnate xenoliths and miarolitic cavities into context of what has already been discovered about the geochronolgy and geochemical characteristics of the Spanish Peaks intrusive suite. The samples collected serve to more broadly understand the implications for the genesis of these rocks as well as of cognate xenoliths and

presence of miarolitic cavities within the radial dikes. These samples are then used in synthesis with other data sets from the Spanish Peaks region in aim to explain the geochemical characteristics of the radial dikes around West Spanish Peak.

**Figure 1.6:** Photo of southwestern flank West Spanish Peak (photo from Johnson, 2014), near the location that the andesitic dike samples were collected from. Here, a radial dike can be seen, on the lower left hand side of the image, heading into West Spanish Peak.

**Figure 1.7:** Photo of sample collection site near where miarolitic cavities and cognate xenoliths were found included into radial dikes (photo from Johnson, 2014). This locale is located near tree-line from the view of the mountain seen in Fig. 1.6, with West Spanish Peak's summit seen in the background.

The analytical methods used to carry out this research project include using a microscope to identify minerals of rock samples under thin section, as well as analytical methods such as using an electron microprobe to determine mineral compositions and an Inductively Coupled Plasma Mass-Spectrometer (ICP-MS) to determine rocks compositions. These analytical techniques provided data about the chemical composition, weight percent oxides, and isotopic ratios within minerals composing the dikes and mountain stock.

Specifically, thin sections were prepared in the Benson Earth Sciences building using a diamond saw to cut rocks down to a manageable size to then be epoxied onto a glass slide. Once firmly attached, the remaining rock piece is ground down to 30 µm thick by hand using 400 and 600 silicon carbide grit. Once thin enough, the thin sections were then polished using a polishing wheel to create smooth surfaces that the electron microprobe can analyze easily. Thin sections were then be analyzed under the

microscope optically in order to determine mineral content, if the material has been altered, or if there are any inclusions in the rock matrix. Once this is completed, the thin sections are mapped optically under the microscope in order to determine specific mineral grains that are polished well enough that they can be probed by the electron microprobe.

The thin sections were taken to the Labratory of Environmental and Geological Sciences (LEGS), and put under the JEOL JXA-8600 superprobe (electron microprobe) to determine spot chemical analysis for those grains identified earlier under the microscope. The electron microprobe's main purpose is that it has the ability to yield specific chemical compositions for an area only a few microns across. The electron microprobe was used to analyze the chemical composition specific mineral phases such as pryoxenes, amphiboles, biotite, feldspars, sulfides, and opaque minerals.

Other rock fragments from the samples collected with be crushed by hand and using a tungsten carbide shatter box, in order to prepare them for whole rock compositional analysis. These crushed powders will be dissolved in HF and other strong acids, then used for Inductively Coupled Mass-Spectrometry (ICP-MS) analysis. Doing this will yield trace element composition for the entire rock, which will then be used to determine if the samples share these compositions or if they are different.

The age of most igneous activity in the West Spanish Peak region ranges from between 26 – 21 million years old, which was determined by Penn (1994), Miggins (2002) , and Penn and Lindsey (2009) using $^{40}Ar/^{39}Ar$ radiometric dating. $^{40}Ar/^{39}Ar$ dating is based on the natural decay of $^{40}K$ to $^{40}Ar$ via the process of electron capture. The basis for this method is the formation of $^{39}Ar$ from $^{39}K$ by bombarding a sample with neutrons. Greater accuracy in dating samples is achieved than conventional $^{40}K/\ ^{40}Ar$ dating because this method measures both parent and daughter isotope abundances at the same time within a single mass spectrometer.

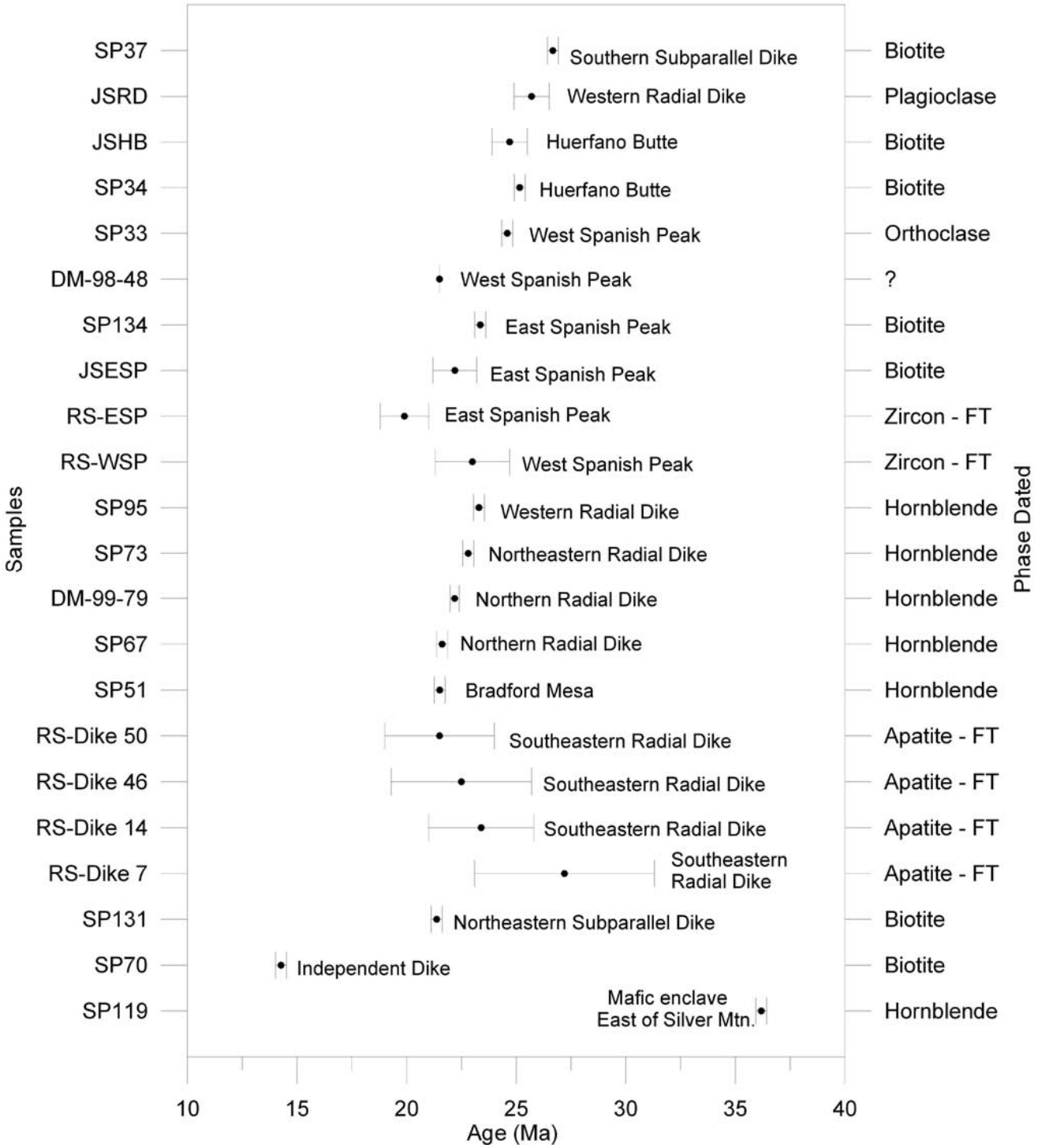


**Figure 1.8:** Geochronological data for Spanish Peaks and nearby rocks compiled by Penn & Lindsey (2009). Samples beginning with: *SP* are from Penn (1994), *RS* are from Smith (1975); *DM* are from Miggins (1999, 2002) and *JS* are from Stormer (1972).

The age of the radial dikes has been confined to within 22 – 23 million years old, and thus the ages for samples of radial dikes collected for this study also fall within this range of dates. Interestingly to note, the date of the West Spanish peak stock falls within 21-25 million years old, and could potentially have formed simultaneously as the genesis of the radial dike swarm around the stock. The close age date-ranges for the radial dikes and the West Spanish Peak stock are one more indication on a temporal scale that these igneous features could possibly share a common magma source based on the timing of their emplacement.

**Table 1.1:** Ages of samples in the West Spanish Peak region, from Smith (1975), Penn (1994) and Miggins (2002), that are similar to samples investigated in this study, ages reported in millions of years ago (M.a.)

| Sample | Sample Type | Source | Age (M.a.) |
|---|---|---|---|
| sp67 | Radial Dike | Penn (1994) | 21.90 |
| sp73 | Radial Dike | Penn (1994) | 22.80 |
| sp95 | Radial Dike | Penn (1994) | 23.30 |
| 98-33 | Radial Dike | Miggins (2002) | 23.46 |
| 98-79 | Radial Dike | Miggins (2002) | 24.19 |
| RS-WSP | WSP Stock | Smith (1975) | 23.00 |
| sp33 | WSP Stock | Penn (1994) | 24.60 |
| 98-48 | WSP Stock | Miggins (2002) | 21.50 |

The samples used in this project come from a variety of studies done in the Spanish Peaks region. Figure 1.8 shows the ensemble of sample locations and the study from which it was originally used in. Samples are broke into four major groupings in order to access the chemical nature of each group and see if there is an established geochemical relationship between these groups as a whole. The four sample groupings are: plutonic stock samples of West Spanish Peak, radial dike samples from around West Spanish Peak, cognate xenoliths samples included into radial dikes, and miarolitic cavitiy samples included within radial dikes. Although the ages have not been determined for each sample individually, age date ranges for samples within each group have been established and it is assumed that other samples within the same group have a comparable age date range. Through establishing the spatial and temporal relationships of these sample groups, a better understanding of the of the Spanish Peaks intrusive suite can be achieved.

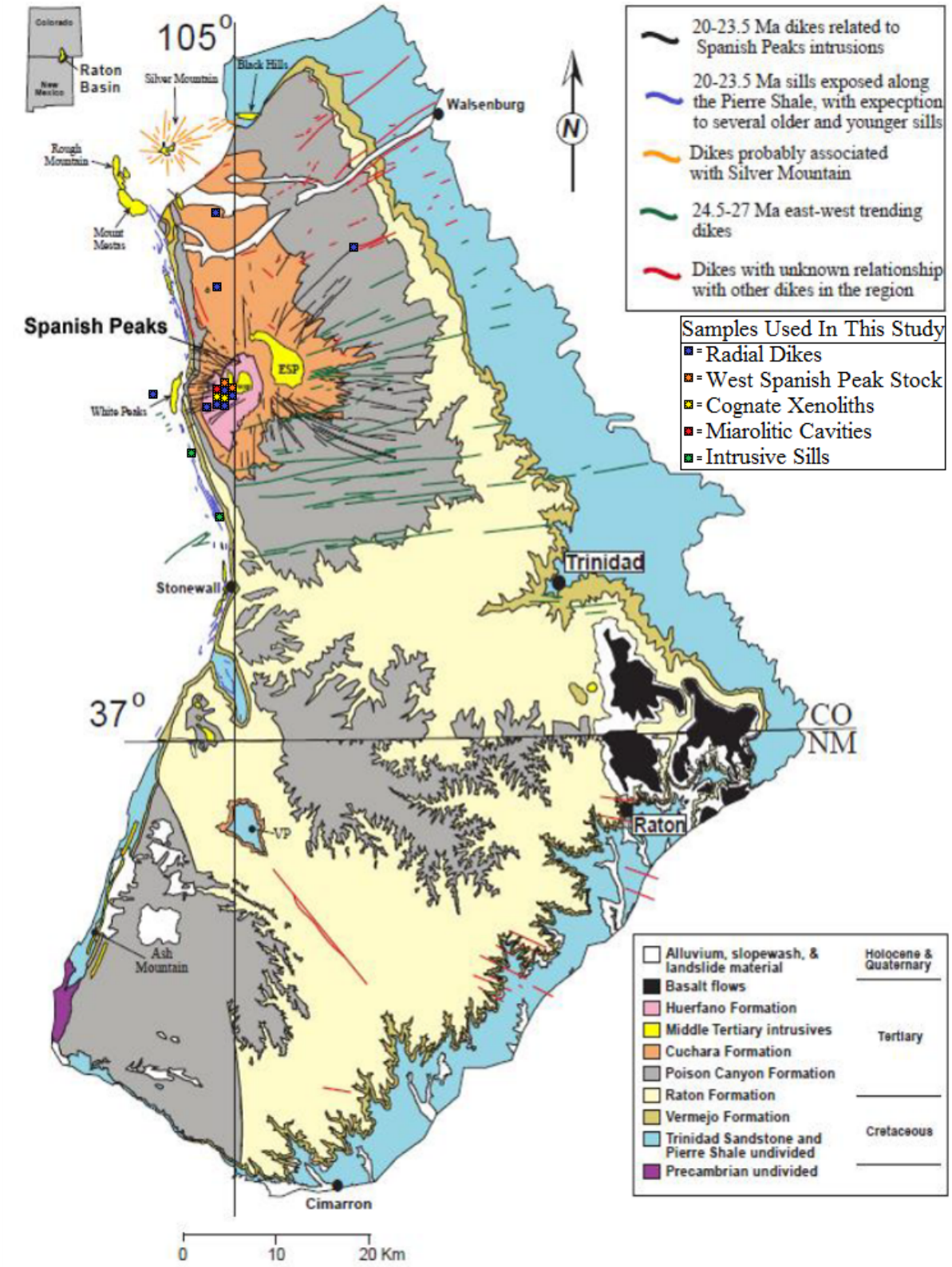


**Figure 1.9:** Geological Map of the Raton Basin from (Miggins, 2002), updated to show locations and original source of samples used in this study. The concentration of samples immediately southwest of West Spanish Peak were collected samples while samples incorporated from other studies are generally more dispersed.

# Chapter 2

## *Petrology*

### Introduction

This chapter is dedicated to describing the mineralogical and textural nature of the West Spanish Peak granitic stock, the surrounding andesitic radial dikes, as well as the cognate xenoliths and miarolitic cavities that are found within those radial dikes. The mineralogy of this set of rocks from the West Spanish Peak area was determined though macroscopic observation of hand samples, as well as observations through a petrographic microscope of thin sections created from those hand samples. The samples included in this study are broken into four distinct groupings based on what they geologically represent. The first two major groupings are the West Spanish Peak stock itself and the surrounding radial dikes. The radial dikes have been found to include cognate xenoliths and miarolitic cavities, as discussed by Contreras (2014) and Johnson (2014), and these compose the third and fourth groups of this study. It is the intention of this chapter to describe each of these groupings, as basis for determining if there is a relationship between them, and to find out whether or not there is a potentially common magma source for all of the discussed features in the West Spanish Peak area.

### West Spanish Peak Stock

The material composing West Spanish Peak (sample IC-16; Fig. 2.1 (i) and (ii)) is a holocrystalline granitic stock composed of euhedral to subhedral grains displaying an equigranular, pheneritic texture. What this all means is that the mineral grains in this rock have roughly the same shape and size of minerals throughout the sample, and they crystallized from a melt that rose relatively quickly and then cooled slowly after it became emplaced into the shallow crust. The majority of the rock is composed of plagioclase feldspar, with less amounts of quartz, potassium feldspar, clinopyroxene, biotite and opaque minerals interspersed throughout, as well as trace amounts of apatite, zircon, and sphene. The abundance of plagioclase feldspar and orthoclase and the presence of quartz are an indication that this sample is intermediate to felsic in its nature.

Based on geochronology work by Penn (1994) and Miggins (2002), the age of West Spanish Peak stock has been constrained to within a range of 22-25 Ma (million years ago). The methodology used to determine this date range, by both Penn (1994) and Miggins (2002), was by using $^{40}Ar/^{39}Ar$

radiometric dating. $^{40}Ar/^{39}Ar$ dating is based on the natural decay of $^{40}K$ to $^{40}Ar$ via the process of electron capture. Greater accuracy in dating samples is achieved than conventional $^{40}K/^{40}Ar$ dating because this method measures both parent and daughter isotope abundances at the same time within a single mass spectrometer.

***Sample IC-16:***

The sample of the West Spanish Peak stock (IC-16; Fig. 2.1 (i) and (ii)) is a weakly altered, holocrystalline rock with a wide mineralogical content ranging from mafic to felsic in nature, but overall represents an intermediate to felsic rock. Approximate mineral abundances within this rock are plagioclase feldspar (30%), orthoclase (20%) clinopyroxene (15%), biotite (15%), quartz (10%), chlorite (5%), as well as opaque and accessory minerals (5%). Plagioclase feldspar dominates this rock sample with the clear, large, subhedral grains present throughout the sample that display lamellar and simple twinning under cross polarized light. Orthoclase, the only alkali feldspar present in this sample, appears as subhedral grains intergrown among sutured plagioclase grains, and displays simple twinning under cross polarized light. Clinopyroxenes are light green to light brown in plane polarized with subhedral grains and are the most altered mineral phase in this sample. Clinopyroxenes in the sample were revealed to be augites under the electron microprobe (Table 3.**x** in Chapter 3). Biotite is light brown to light orange in plane polarized light, with generally subhedral grains. Quartz, appears infrequently and commonly displays clear, unaltered, anhedral grains. Chlorite is present in this sample, appears in amorphous masses as an alteration phase, usually the expense of cliopyroxene grains. Opaque minerals are minor phases in the sample, and appear in higher concentrations in areas that are altered to chlorite.

This rock at first glance seems to represent a typical granite, however the quartz content is too low to be considered a granite. Thus, this rock is closer to a quartz monzonite, which is a plutonic rock in between intermediate and felsic mineralogy. The abundance of plagioclase and clinopyroxene are the largest indicators that this rock is otherwise still of at least intermediate mineralogy. Clinopyroxenes are not found typically found in highly felsic environments, but can form in diorites which are the intermediate plutonic equivalent of an andesite. Besides the deficiency of quartz, the presence of clinopyroxene is another reason why this rock shows a more intermediate mineralogy than a typical granite.

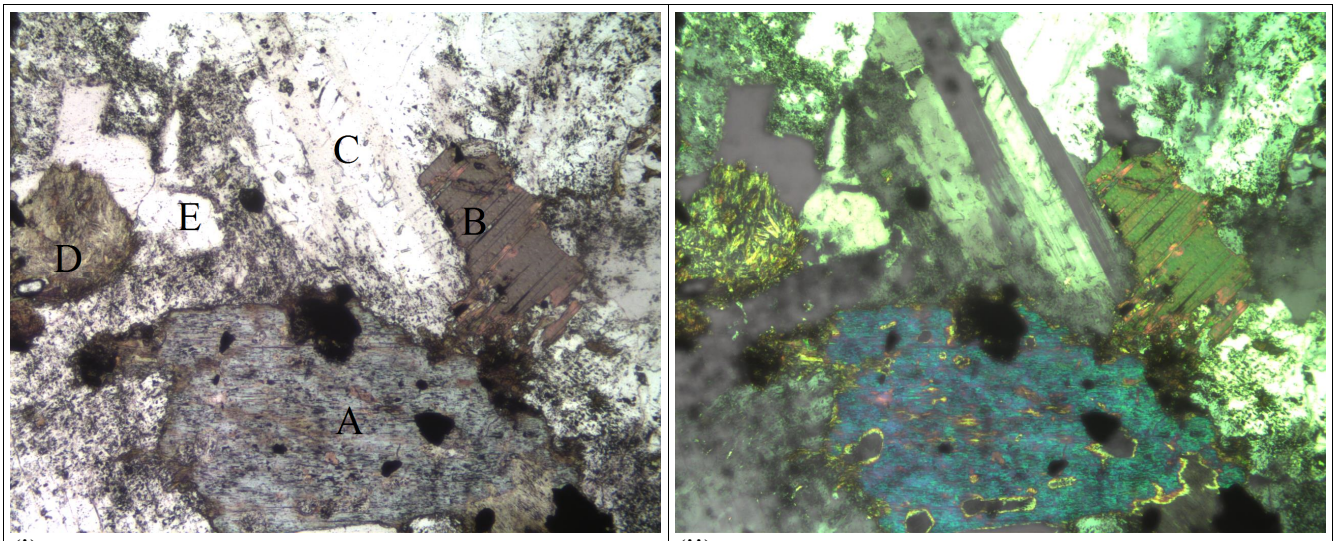


(i) (ii)

**Figure 2.1 (i) and (ii):** Sample IC-16 at 60 times magnification (4x zoom multiplied by 15x ocular) in plane polarized light (i) and in cross polarized light (ii). (A) A large, green, phenocryst of clinopyroxene; (B) a brown biotite phenocryst; (C) A large clear phenocryst of plagioclase feldspar; (D) a cliopyroxene mass being altered to chlortie. (E) A clear quartz phenocryst. Opaques compose the dark patches of minerals.

By using an electron microprobe, it was determined that the oxide minerals composing the opaques in this sample are a combination of mostly illmenite with some titanomegnetite and hematite also present. In addition to this, we also found in one instance that an additional sulfide, pyrite, was present. The presence of both illmenite and titanomagnetite in this sample is interesting because illmenite is primarily found in alkaline environments, while titanomagnetite is primarily found in calc-alkaline environments. What this says about the formation of West Spanish peak is that, there might have been a transition from and alkaline environment to a sub-alkaline environment while the granitic stock was crystallizing. This idea is explored further in Chapter 3 (Mineral Chemistry).

**Radial Dikes**

Overall, the radial dikes around West Spanish Peak appear to be hypocrystalline, displaying subhedral phenocryst grains, and a porphyritic texture, meaning that larger crystal grains are embedded within a matrix of a fine grained ground-mass. Based on the array of minerals present, this suite of rocks is andesitic. There are some variations in the mineralogy of each dike, what oxide phases and trace minerals are present, as well as what the degree of alteration is. There are three dike samples and descriptions listed in this study, and they intend to build on the understanding of the radial dikes

hosting cognate xenoliths and miarolitic cavities as described by Contreras (2014) and Johnson (2014).

Based on geochronology work by Penn (1994) and Miggins (2002), the age of five radial dikes around West Spanish peak has been confined to within an age date range of 22-24 Ma. The methodology used to determine this date range, by both Penn (1994) and Miggins (2002), was again by using $^{40}Ar/^{39}Ar$ radiometric dating. The close age date-ranges for the radial dikes and the West Spanish Peak stock might allude to a co-genetic relationship, another indication that igneous features in this region potentially share a common magma source..

Through use of an electron microprobe, it was determined that two of the three samples described below, SR-7 and SR-8b, also contain both the oxide mineral phases illmenite and titanomagnetite. Similarly to the West Spanish peak stock, the presence of both illmenite and titanomagnetite in this sample is interesting because illmenite is primarily found in alkaline environments, while titanomagnetite is primarily found in calc-alkaline environments. The presence of both of these oxides are also found in the West Spanish peak stock, and the implications of this are that there might have been a transition from and alkaline environment to a sub-alkaline environment while the granitic stock was crystallizing, and this is further discussed in Chapter 3 (Mineral Chemistry).

***Sample SR-7:***

This radial dike sample (sample SR-7; Fig. 2.2 (i) and (ii)) is a hypocrystalline rock composed of relatively unaltered intermediate mineralogy and displays a porphyritic texture. The mineral abundances of this dike are plagioclase feldspar (55%), clinopyroxene (35%), and opaques and accesory minerals (10%). Plagioclase phenocrysts are generally clear anhedral grains that show lamellar twinning under cross polarized light. Plagioclase phenocrysts are also often altered and show a fiberous texture with relict twinning remaining, however the dike's other mineral phases are still relatively unaltered. Clinopyroxene grains are clear to light green under plane polarized light, and many unaltered, euhedral to subhedral phenocrysts can be found. The opaque minerals are throughout the sample, which is another indication that this sample is relatively unaltered due to weathering and surface processes.

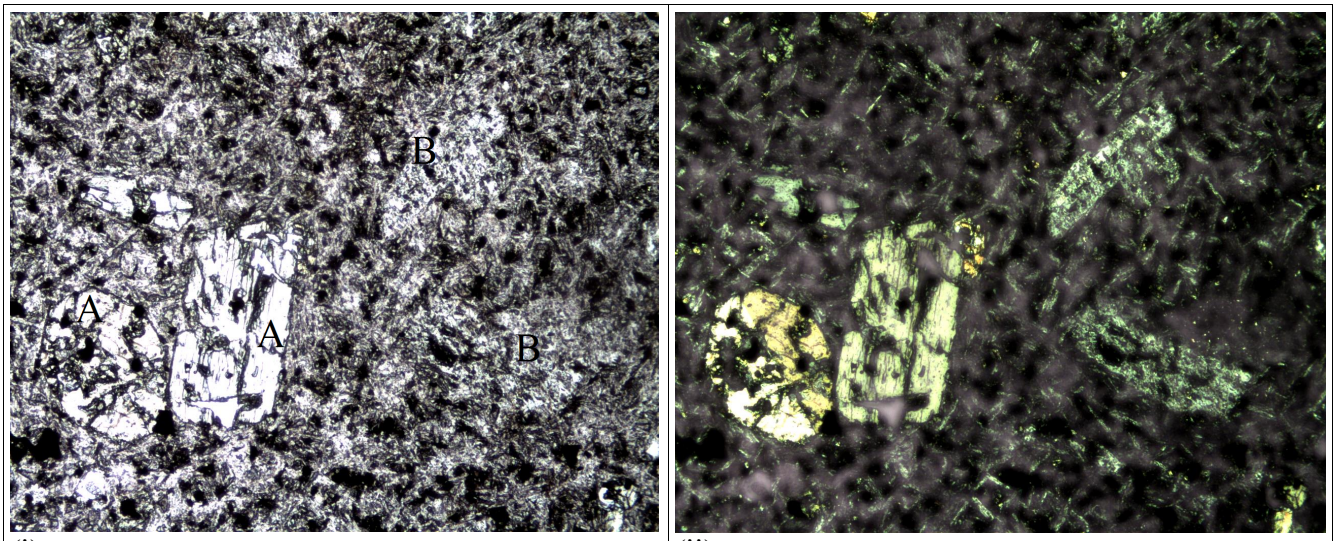


(i) (ii)

**Figure 2.2 (i) and (ii):** Sample SR7 at 60 times magnification (4x zoom multiplied by 15x ocular) in plane polarized light (i) and in cross polarized light (ii). (A) Two moderately altered large phenocrysts of cliopyroxene; (B) Highly altered plagioclase phenocrysts containing air bubbles within them. Opaque minerals compose the dark patches.

The abundance of clinopyroxene in this sample is an indication that the magma still contains mineral phases the crystallized at higher temperatures and pressures. The ground mass of the dike is composed of primarily very small plagioclase grains, but is also accompanied by a fair share of clinopyroxene grains and opaque minerals. Both the texture and mineral composition of this rock most closely resemble and andesite, an intermediate rock with a porphyritic texture. The dike also contains small miarolitic cavities where volatiles existed within the melt as it cooled. These small cavities have since been partially filled in by quartz and calcite that were deposited via groundwater.

***Sample SR-8b:***

The radial dike (sample SR-8b; Fig. 2.3 (i) and (ii)) is a hypocrystalline rock displaying an intermediate mineralogy, and a porphyritic texture. Additionally, this dike is an example of a host dike in which large miarolitic cavities are found, as also discussed by Johnson (2014). The abundance of minerals in this rock is roughly plagioclase feldspar (40%), clinopyroxene (25%), amphibole (15%), quartz (10%), chlorite and accessory minerals (5%), and opaques (5%). The plagioclase feldspar phenocrysts in this sample are relatively unaltered, clear, anhedral grains that display lamellar twinning in grains of sufficient size. The clinopyroxene phenocrysts are clear to light green under plane polarized light, and are relatively unaltered, subhedral grains. Some clinopyroxenes in this sample

dsisplay simple twinning under cross polarized light. The amphibole in this sample tends to primarily form in large, subhedral phenocrysts, ranging from light brown to dark brown under plane polarized light. Quartz is rare in this sample, but when present is euhedral to subherdal grains. Chlorite is also present in this sample appearing to be present in highly altered portions of larger plagioclase, pyroxene and amphibole phenocrysts.

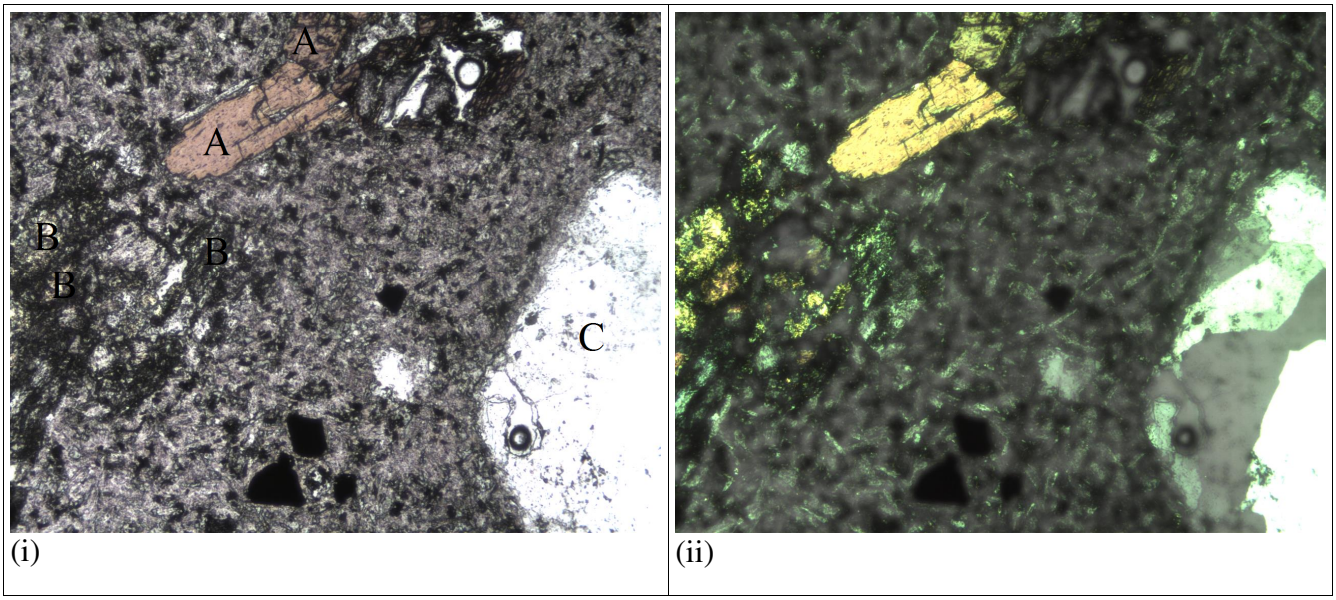


**Figure 2.3 (i) and (ii):** Sample SR8b at 60 times magnification (4x zoom multiplied by 15x ocular) in plane polarized light (A) and in cross polarized light (B). (A) A large brown amphibole phenocryst; (B) An altered clinopyroxene phenocryst; (C) An unaltered quartz phenocryst. Opaque minerals compose the dark patches of minerals.

The presence of clinopyroxene and amphibole in this sample is an indication that the magma contains mineral phases that crystallized at higher temperatures and pressures. The matrix of this sample contains an abundance of very small plagioclase grains along with portions of clinopyroxene and opaque mineral phases. Both the texture and mineral composition of this rock indicate this rock resembles an andesite, an intermediate rock with a porphyritic texture. The dike also contains large miarolitic cavities: pockets of air in which gas bubbles once existed as the magma that formed the dike cooled. These pockets have since filled in by minerals that were deposited by groundwater after the dike formed.

***Sample IC-SPD4:***

This radial dike (sample IC-SPD4; Fig. 2.4 (i) and (ii)) is a hypocrystalline rock displaying and

a porphyritic texture. Also, it is important to note that this radial dike is an example of the host dike in which the cognate xenoliths are found, as discussed by Contrereas (2014). Mineral abundances in this sample occur to appear to be plagioclase feldspar (45%), clinopyroxene (25%), amphiboles (20%), opaques (10%), and chlorite and accessory minerals (5%). The plagioclase feldpsar phenocrysts in this sample are clear, unaltered, euhedral grains displaying lamellar twinning, as well as occasional simple twinning under cross polarized light. It is important to note that the plagioclase in this sample also often displays chemical zonation. Clinopyroxene phenocrysts in this sample ranges from light green to dark green in plane polarized light, and generally displays unaltered euhedral to subhedral grains. Amphiboles phenocrysts in this sample range from light to dark brown under plane polarized light, and display generally subhedral, unaltered grains. Chlorite appears in the sample as an alteration phase that appears to consume very small portions of pyroxene and plagioclase grains. The matrix of this dike is also relatively unaltered, and is composed of primarily very small plagioclase, clinopyroxene and opaque grains.

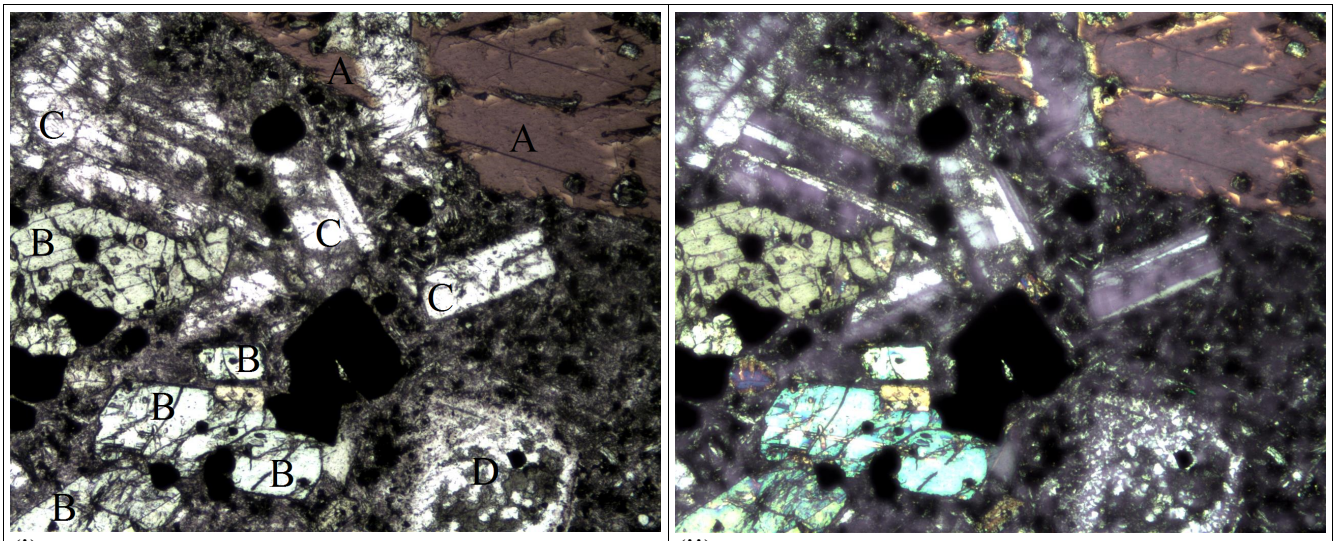


(i) (ii)

**Figure 2.4 (i) and (ii):** Sample IC-SPD4 at 60 times magnification (4x zoom multiplied by 15x ocular) in plane polarized light (A) and in cross polarized light (B). (A) large brown phenocryst of amphibole; (B) The pale green phenocrysts are clinopyroxenes; (C) The strip of clear phenocrysts are all plagioclase feldspars; (D) Clinopyroxene that has been altered to chlorite. Opaques compose the park patches of minerals.

The presence of subhedral amphiboles is the strongest indication on a macroscopic scale that this dike likely shares a common magma source as the cognate xenoliths. In comparison of overall mineralogy of the cognate xenoliths compared to the mineralogy of this dike, this dike tends to have a

higher abundance of plagioclase included than inside the xenoliths. That said, the mineral phases in this radial dike correspond almost exactly to the minerals that compose the xenoliths, and thus it is possible that a relationship may exist between the source of these two features.

## Cognate Xenoliths

Some of the radial dikes around West Spanish Peak include xenoliths, which are foreign pieces of rock, incorporated into the radial dikes. Macroscopically the xenoliths are dark in color, with generally larger grains that the groundmass and phenocrysts found within the dikes. The xenoliths do not bear any resemblance to the West Spanish Peak stock either, as they are also textually very different from one another. Minerals found within the xenoliths include plagioclase feldaspar, clinopyroxene, amphiboles, as well as opaque minerals and trace amounts of apatite. Generally, the xenoliths are darker in color and exhibit larger crystals of more mafic minerals than either the radial dikes or West Spanish peak stock. The xenoliths are also mostly comprised of large unaltered grains of amphiboles and clinopyroxenes, with plagioclase playing a more intermediate role. In contrast, the dikes which host these xenoliths, are comprised of primarily plagioclase feldspar, with more mafic minerals such as amphibole and clinopyroxene composing smaller amounts of the rock. The mineralogy of the xenoliths also contrasts with the composition of the West Spanish Peak stock, which is composed of mostly plagioclase feldpsar and potassium feldspar, along with quartz, with more mafic minerals such as clinopyroxene and biotite making up smaller amounts of the rock.

As for the age of these xenoliths, no specific geochronology work was done to determine their age in this study, however because these features are found within the radial dikes surrounding West Spanish Peak, it can be assumed that their incorporation into the dike material is comparable to the age of the radial dike swarm. Thus, the age of the cognate xenoliths is assumed to be within the age date range of 22-23 Ma, based on geochronology work by Penn (1994) and Miggins (2002).

### *Sample IC-7:*

The first cognate xenolith examined in this study (sample IC-7; Fig. 2.5 (i) and (ii)) is holocrystalline, with generally very large, relatively unaltered, euhedral to subhedral grains and display a pheneritic, equigranular texture. This sample's mineral abundances are approximately: amphibole (40%), plagioclase feldspar (40%), opaques (>15%) and trace amounts of clinopyroxene and apatite (<5%). Amphiboles range from a light tan to dark brown in color, while the shape of crystal gains is

generally euhedral to subhedral. In nearly equal proportion, is plagioclase feldspar, displaying large, clear, euhedral to subhedral grains that demonstrate both simple and lamellar twinning under cross polarized light. Plagioclase grains also appear to show chemical zonation in some grains as well. Opaque minerals appear sporadically in between large sutured amphibole and plagioclase grains. Opaque mineral crystals appear to be larger in this samples than in other xenolith samples examined in this study.

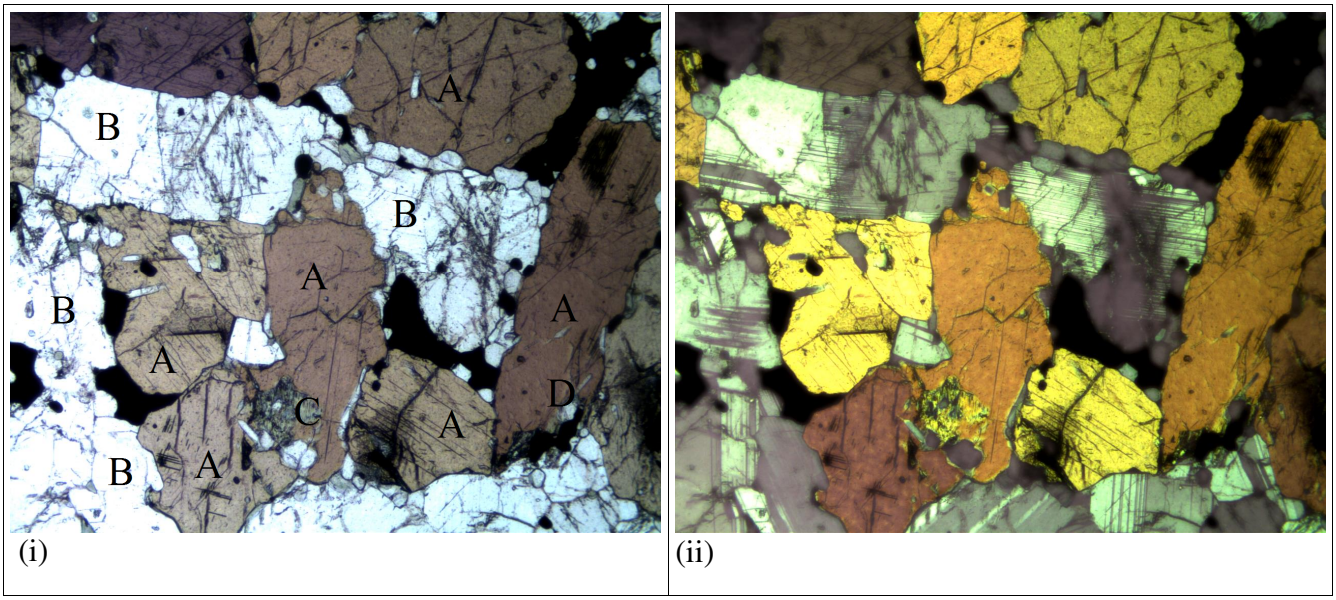


**Figure 2.5 (i) and (ii):** Sample IC-7 at 60 times magnification (4x zoom multiplied by 15x ocular) in plane polarized light (i) and in cross polarized light (ii). (A) Large, brown phenocrysts throughout the image are amphiboles; (B) Large, clear phenocrysts throughout the image are plagioclase feldspars; (C) Former Chliopyroxene grain that has been altered to chlorite; (D) Apatite can be seen growing within amphibole phenocrysts Opaques compose the dark patches in between amphibole and plagioclase..

The most interesting thing to remark on about this sample is the absence of clinopyroxene of any noteworthy size or abundance. If it is present at all within the xenolith at all, it is almost entirely altered to chlorite. It is also important to note that there is a smaller proportion of alteration and alteration phases present in comparison to other xenolith samples. This is interesting to note because larger degrees of alteration, and alteration phases such as chlorite, are found within the host dikes that the xenoliths are incorporated into. According to Contreras (2014), the opaque minerals present in this sample are titanomagnetites, as revealed through use of the electron microscope.

***Sample IC-14a:***

The other cognate xenolith incorporated in this study (sample IC-14a; Fig. 2.6 (i) and (ii)) is also holocrystalline, with mildly altered, very large, subhedral grains and displays a phaneritic, equigranular texture. This sample's mineral abundances are approximately: amphibole (45%), clinopyroxene (45%), chlorite (5%), and opaques (5%). Amphiboles range from light tan to medium brown, and generally have large, subhedral grains. In areas where the amphibole is highly weak or fractured it appears that the amphibole has altered to chlorite in these areas. In roughly the same proportion, clinopyroxene grains are also generally large and subhedral in shape, often altered to chlorite in highly fractured places. Opaque minerals and chlorite are present in the areas that appear to be most highly altered, such as in large cracks or holes within amphibole and clinopyroxene phenocrysts.

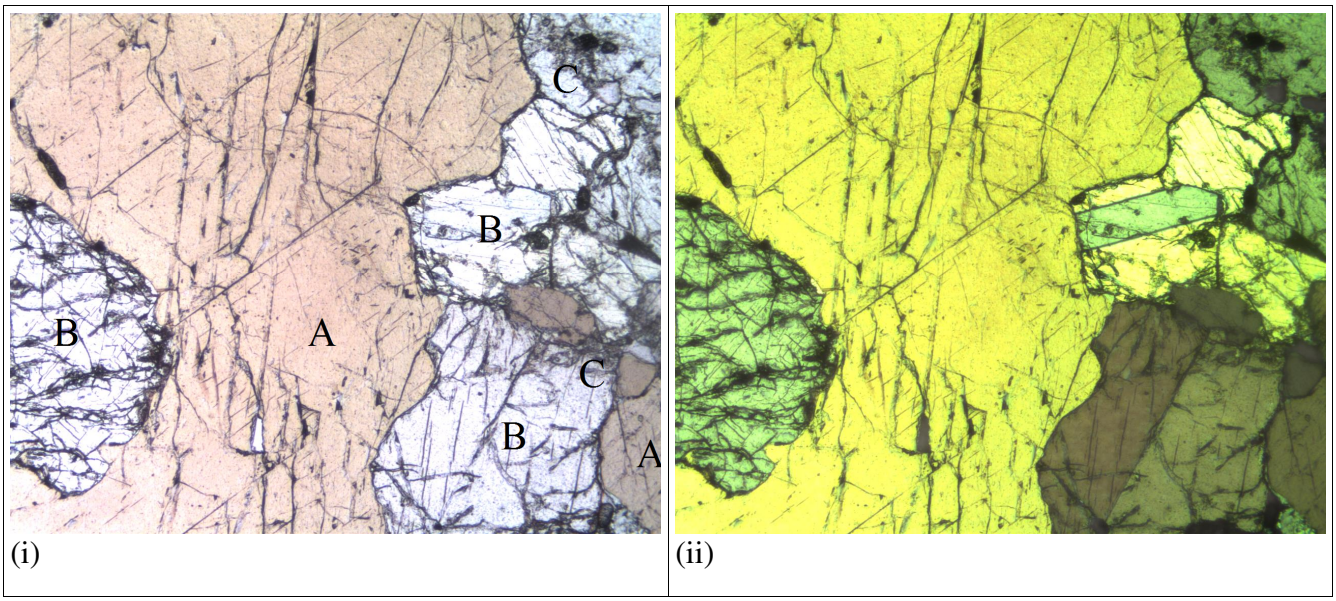


**Figure 2.6 (i) and (ii):** Sample IC-14a at 60 times magnification (4x zoom multiplied by 15x ocular) in plane polarized light (i) and in cross polarized light (ii). (A) Brown amphibole phenocrysts; (B) Large, pale green to clear, clinopyroxene phenocrysts; (C) Chlorite is filling in gaps in between amphibole and clinopyroxene as well as in areas of high alteration. Opaque minerals are also seen as dark patches in alteration areas.

This sample is notably absent of plagioclase feldpsar of any distinguishable size or abundance. This sample in also particularly interesting because it holds roughly equal proportions of amphibole and clinopyroxene, which is a higher amount of clinopyroxene than typically associated with other cognate xenolith samples described by Contereas (2014). Opaque mineral phases and chlorite appear to fill in any gaps created in between amphibole and clinopyroxene phenocrysts.

**Miarolitic Cavities**

Miarolitic is a term that describes cavities lined with crystals of various mineral phases that can be found in igneous rocks. Cavities that are miarolitic in nature contain entrapped mineral rich fluids derived from granitic magma that has been segregated due to fractional crystallization during the final stages of crystallization. The environment miarolitic cavities are most closely associated with is granitic pegmatites, which are holocrystalline, intrusive, felsic igneous rocks. In general, many miarolitic cavities contain both minerals associated with granitic, or felsic, environments, as well as accessory minerals resulting from the concentration of trace-elements due to hydrothermal activity. Examples of minerals commonly found within miarolitic cavities are: quartz, feldspars, tourmaline, flourite, and other hydrothermal mineral phases. The minerals that end up precipitating into miarolitic cavities depend on a variety of factors including: the composition of the source rock, amount of volatiles present, and the pressure and temperature conditions under which the melt crystallized under. The study of miarolitic cavities thus in turn reveals information about the conditions required to produce the melt from which they formed.

In the context of this project, the aim of studying the miarolitic cavities found in the radial dikes around West Spanish peak will reveal information about the conditions under which the dike swarm cooled. The mineral phases detected within miarolitic cavities in the radial dikes around West Spanish Peak are primarily composed of quartz, epidote, and chlorite; with trace amounts of muscovite, clacite, barite, and opaque mineral phases. Using an electron microprobe it was determined that the opaque mineral phases included within the miarolitic cavities include: both botryoidal and platy hematite, pyrite, chalcopyrite, and in one case a coblate sulfate called carrolite.

This study incorporates the first isotopic work done on miarolitic cavities in the Spanish Peaks area, and used strontium isotope values to determine whether the miarolitic cavities were formed during the crystallization of the melt,.or were later deposited by the precipitation of groundwater in a hydrothermal setting. Based on the isotopic work completed, later discussed in Chapter 3, it has been determined that the presence of miarolitic cavities found within the radial dikes around West Spanish Peak are associated with precipitation due to groundwater passing through the radial dikes, rather than crystallization directly from the melt that also composes the radial dikes. As for the ages of the miarolitic cavities, although no specific geochronology work has been done to determine the ages of these features, it assumed that their deposition is associated with paleo-groundwater events that passed through the radial dikes surrounding West Spanish Peak. Therefore, it is speculated that the oldest ages

of the miarolitic cavites could be contemporaneous with the ages of the radial dikes, 22-23 Ma based on the geochronolgy work done by Penn (1994) and Miggins (2002), with no lower bound to how young they might be. To determine the exact ages of the miarolitic cavities, future isotopic work could be done to determine the timing of such a paleo-groudwater event.

***Sample TJ-2a:***

The sample of a miarolitic cavity included into this project (sample TJ-2a; Fig. 2.7 (i) and (ii)) is an example of a relative large miarolitic cavity included into the groundmass of a radial dike that was found on the southwestern flank of West Spanish peak. The radial dike is very similar in regard to other radial dike samples described previously in this study. There is a groundmass composed of primarily plagioclase feldspar, clinopyroxene, and opaque minerals surrounding the miarolitic cavity. However unlike the radial dikes already described, large phenocrysts of plagioclase and amphibole have been highly altered to chlorite and epidote. The miarolitic cavity itself consists from the edge inwards intergrown rims of the specific mineral phases towards the center, in this order: quartz, epidote, chlorite, calcite, barite, and then opaque minerals. The group of opaque minerals in this sample is diverse, and represents a range of metallic cations contained within the fluid from which the minerals in these cavities precipitated from. The opaque mineral phases detected using an electron microprobe include: pyrite, chalcopyrite, hematite, and the cobalt sulfide carrollite, and the presence of this suite of opaques if further discussed in the mineral chemistry chapter (Chapter 3).

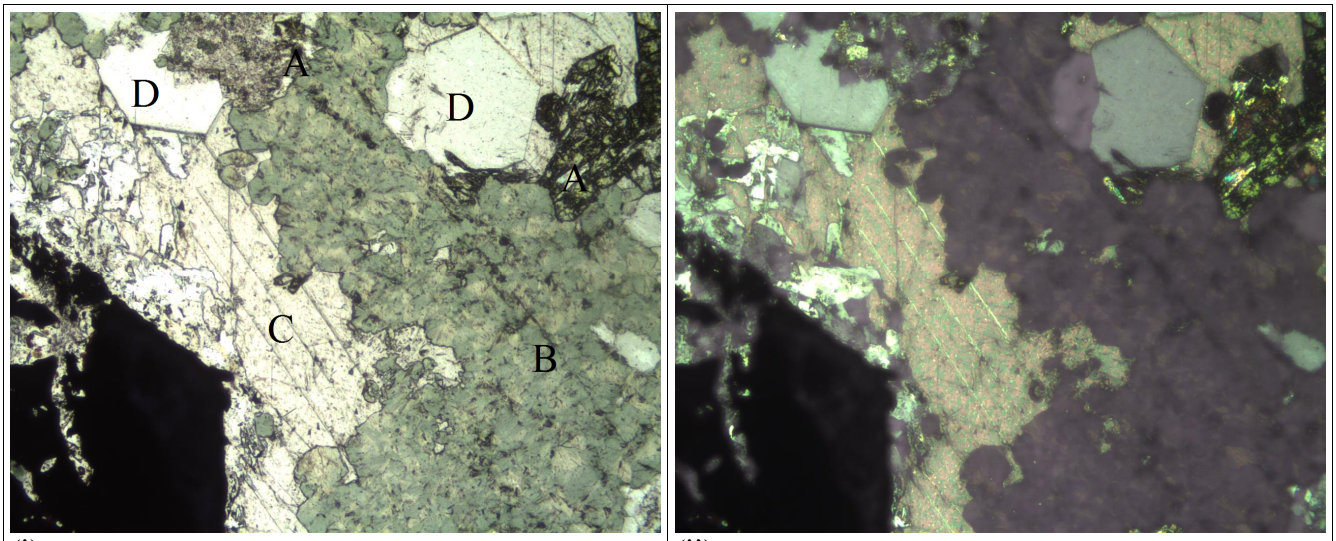


(i) (ii)

**Figure 2.7 (i) and (ii):** Sample TJ-2a at 60 times magnification (4x zoom multiplied by 15x ocular) in plane polarized light (i) and in cross polarized light (ii). (A) Bright green minerals in top-right are epidote. (B) Pale green seen on right are chlorite masses. (C) Clear mineral in center of the image surrounding the opaque mass is calcite; (D) Clear grain in the top-right is quartz. Opaque mass is the dark mass in the lower-left portion of the screen.

# Chapter 3

## *Mineral Chemistry*

## Introduction

Mineral chemistry for clinopyroxene, amphiboles, plagioclase feldspars, biotite, and opaque minerals (sulfides, and oxides) in a total of seven samples were determined using electron microprobe analysis. Samples analyzed by the electron microprobe to be included in this study are as follows: one from the West Spanish Peak plutonic stock (sample IC-16), three radial dikes (samples SR-7, SR-8b and IC-SPD4), two cognate xenoliths (samples IC-7 and IC-14a) were and one miarolitic cavity (sample TJ-2a). Analytical results from the electron microprobe are displayed in Tables 3.1 through 3.13

## Clinopyroxene

Clinopyroxene was identified and analyzed in the Spanish Peak stock (sample IC-16), two radial dikes (samples SR-7 and IC-SPD4) and one cognate xenolith (sample IC-14a) sample. Augite and diopside have been identified to exist within the West Spanish Peak intrusive complex. Augite is relatively iron rich in comparison to diopside, while diopside has relatively more calcium and magnesium than most augites.

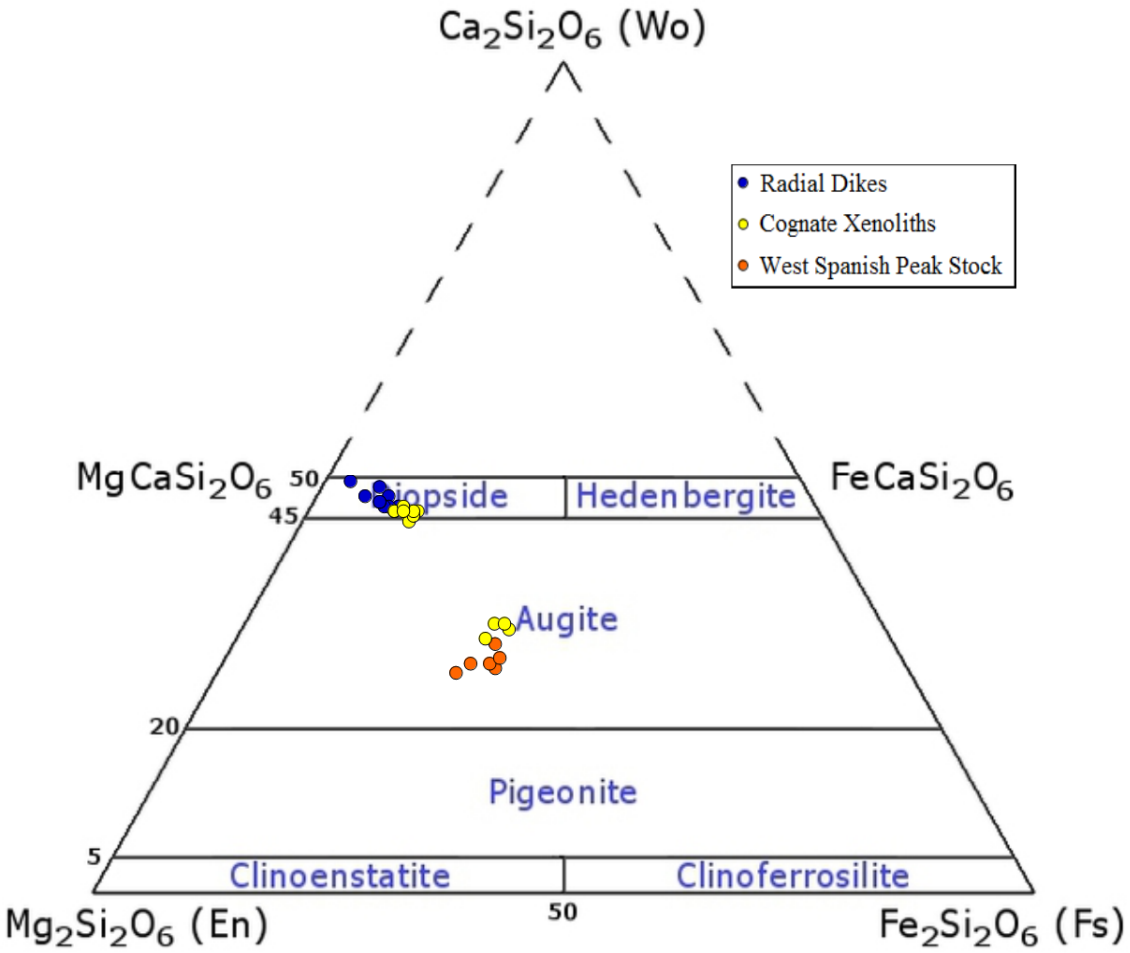


**Figure 3.1:** Plot of pyroxene variation between West Spanish Peak stock, a radial dike hosting xenoliths, and cognate xenolith samples. Cognate xenoliths and host radial dike plagioclase values are reported from Contreras (2014). Note that plagioclase-amphibole rich xenoliths contain augite like the West Spanish Peak stock, while the pyroxene-amphibole rich xenoliths contain diopside similar to the radial dike swarm. Axes are in Mol. Precentage.

***West Spanish Peak***

West Spanish peak's stock (sample IC-16) contains the variety of pyroxene called augite, a clinopyroxene that contains relatively low amounts of calcium and magnesium while being slightly enriched in iron. Weight percent oxides for calcium range from 10.72 – 11.85 percent. Weight percent oxides for magnesium range from 12.52 – 15.46 percent. And weight percent oxides for iron range from 13.12 – 17.01 percent.

**Table 3.1:** Clinopyroxene electron probe oxide data for the West Spanish Peak stock (sample IC-16).

| Sample: | IC-16 | | | | | |
|---|---|---|---|---|---|---|
| | Augite 1 | Augite 2 | Augite 3 | Augite 4 | Augite 5 | Augite 6 |
| $SiO_2$ | 53.26 | 53.90 | 53.20 | 51.25 | 52.76 | 51.90 |
| $TiO_2$ | 0.10 | 0.14 | 0.29 | 0.29 | 0.26 | 0.22 |
| $Al_2O_3$ | 0.90 | 0.72 | 1.98 | 2.47 | 1.42 | 1.93 |
| $Cr_2O_3$ | 0.00 | 0.00 | 0.01 | 0.02 | 0.19 | 0.00 |
| *FeO | 16.07 | 13.12 | 14.95 | 16.87 | 17.01 | 15.94 |
| MnO | 0.38 | 0.43 | 0.43 | 0.41 | 0.45 | 0.33 |
| MgO | 13.00 | 15.46 | 14.96 | 12.52 | 13.08 | 13.04 |
| CaO | 11.85 | 11.29 | 10.72 | 11.11 | 11.03 | 11.53 |
| $Na_2O$ | 0.22 | 0.14 | 0.40 | 0.49 | 0.28 | 0.35 |
| $K_2O$ | 0.08 | 0.05 | 0.16 | 0.22 | 0.15 | 0.17 |
| Total | 95.86 | 95.23 | 97.06 | 95.65 | 96.45 | 95.42 |
| Number of Ions based on 6 Oxygen | | | | | | |
| Si | 2.07 | 2.07 | 2.03 | 2.01 | 2.04 | 2.03 |
| Ti | 0.00 | 0.00 | 0.01 | 0.01 | 0.01 | 0.01 |
| Al | 0.04 | 0.03 | 0.09 | 0.11 | 0.07 | 0.09 |
| Cr | 0.00 | 0.00 | 0.00 | 0.00 | 0.01 | 0.00 |
| Fe | 0.52 | 0.42 | 0.48 | 0.55 | 0.55 | 0.52 |
| Mn | 0.01 | 0.01 | 0.01 | 0.01 | 0.02 | 0.01 |
| Mg | 0.75 | 0.88 | 0.85 | 0.73 | 0.76 | 0.76 |
| Ca | 0.49 | 0.47 | 0.47 | 0.47 | 0.46 | 0.48 |
| Na | 0.02 | 0.01 | 0.03 | 0.04 | 0.02 | 0.03 |
| K | 0.00 | 0.00 | 0.01 | 0.01 | 0.01 | 0.01 |
| Total | 3.92 | 3.91 | 3.94 | 3.95 | 3.93 | 3.94 |

***Radial Dikes***

Analyses of two radial dikes (samples SR-7 and IC-SPD4) show that the radial dikes contains the variety of pyroxene called diopside, a clinopyroxene that contains relatively low amounts of iron while being slightly enriched in calcium and magnesium. Weight percent oxides for calcium range from 19.75 – 21.98 percent. Weight percent oxides for magnesium range from 13.3 – 15.52 percent. And weight percent oxides for iron range from 5.68 – 8.91 percent.

**Table 3.2:** Clinopyroxene electron probe oxide data for radial dikes surrounding West Spanish Peak (samples

SR-7 and IC-SPD4).

| **Sample:** | **SR-7** | | | | | | | **IC-SPD4** | | | |
|---|---|---|---|---|---|---|---|---|---|---|---|
| | Diopside 1 | Diopsie 2 | Diopside 3 | Diopside 4 | Diopside 5 | Diposide 6 | Diopside 7 | Diopside 1 | Diopside 2 | Diopside 3 | Diopside 4 |
| $SiO_2$ | 51.59 | 50.01 | 50.13 | 49.79 | 50.81 | 51.21 | 51.58 | 48.28 | 51.52 | 50.80 | 50.92 |
| $TiO_2$ | 0.92 | 1.03 | 0.99 | 0.94 | 0.95 | 0.70 | 0.53 | 1.21 | 0.55 | 0.76 | 0.66 |
| $Al_2O_3$ | 2.55 | 4.05 | 2.97 | 2.80 | 2.50 | 1.71 | 1.67 | 6.55 | 2.56 | 3.76 | 2.88 |
| $Cr_2O_3$ | 0.00 | 0.18 | 0.01 | 0.00 | 0.00 | 0.00 | 0.00 | 0.12 | 0.19 | 0.22 | 0.00 |
| *FeO | 8.21 | 6.88 | 7.39 | 7.72 | 8.84 | 8.91 | 8.76 | 7.15 | 8.26 | 5.68 | 8.24 |
| MnO | 0.23 | 0.12 | 0.25 | 0.20 | 0.20 | 0.40 | 0.32 | 0.11 | 0.53 | 0.06 | 0.40 |
| MgO | 15.52 | 15.01 | 14.59 | 14.59 | 14.68 | 13.8 | 14.09 | 13.3 | 14.32 | 15.24 | 13.65 |
| CaO | 19.82 | 19.97 | 20.68 | 20.45 | 20.46 | 19.75 | 20.01 | 21.98 | 20.18 | 21.92 | 20.76 |
| $Na_2O$ | 0.49 | 0.48 | 0.45 | 0.45 | 0.46 | 0.61 | 0.60 | 0.43 | 0.58 | 0.39 | 0.60 |
| $K_2O$ | 0.01 | 0.01 | 0.02 | 0.01 | 0.00 | 0.00 | 0.00 | 0.01 | 0.00 | 0.07 | 0.00 |
| Total | 99.34 | 97.74 | 97.48 | 96.94 | 97.89 | 97.08 | 97.55 | 99.14 | 98.7 | 98.84 | 98.1 |
| Number of Ions based on: 6 Oxygen | | | | | | | | | | | |
| Si | 1.92 | 1.89 | 1.91 | 1.10 | 1.91 | 1.96 | 1.97 | 1.81 | 1.94 | 1.89 | 1.93 |
| Ti | 0.03 | 0.03 | 0.03 | 0.03 | 0.03 | 0.02 | 0.02 | 0.03 | 0.02 | 0.02 | 0.02 |
| Al | 0.11 | 0.18 | 0.20 | 0.13 | 0.11 | 0.08 | 0.08 | 0.30 | 0.11 | 0.17 | 0.013 |
| Cr | 0.00 | 0.01 | 0.00 | 0.00 | 0.00 | 0.00 | 0.00 | 0.00 | 0.01 | 0.01 | 0.00 |
| Fe | 0.26 | 0.22 | 0.24 | 0.25 | 0.28 | 0.29 | 0.28 | 0.22 | 0.26 | 0.18 | 0.26 |
| Mn | 0.01 | 0.00 | 0.01 | 0.01 | 0.01 | 0.01 | 0.01 | 0.00 | 0.02 | 0.00 | 0.01 |
| Mg | 0.86 | 0.84 | 0.83 | 0.83 | 0.82 | 0.79 | 0.80 | 0.74 | 0.80 | 0.85 | 0.77 |
| Ca | 0.79 | 0.81 | 0.84 | 0.84 | 0.83 | 0.81 | 0.82 | 0.88 | 0.81 | 0.88 | 0.84 |
| Na | 0.04 | 0.04 | 0.03 | 0.03 | 0.03 | 0.05 | 0.04 | 0.03 | 0.04 | 0.03 | 0.04 |
| K | 0.00 | 0.00 | 0.00 | 0.00 | 0.00 | 0.00 | 0.00 | 0.00 | 0.00 | 0.00 | 0.00 |
| Total | 4.01 | 4.01 | 4.02 | 4.02 | 4.02 | 4.00 | 4.01 | 4.02 | 4.01 | 4.02 | 4.01 |

***Cognate Xenolith***

The analysis shows that the cognate xenolith (sample IC-14a) analyzed contains diopside as the only type of pyroxene present. Weight percent oxides for calcium range from 11.09 – 21.01 percent. Weight percent oxides for magnesium range from 13.17 – 14.30 percent. And weight percent oxides for iron range from 7.84 – 11.27 percent.

**Table 3.3:** Clinopyroxene electron probe data for a cognate xenolith found within a radial dike (sample IC-14a).

| **Sample:** | **IC-14a** | | |
|---|---|---|---|
| | Diopside 1 | Diopside 2 | Diopside 3 |
| $SiO_2$ | 51.60 | 51.52 | 51.99 |
| $TiO_2$ | 0.66 | 0.65 | 0.41 |
| $Al_2O_3$ | 3.74 | 3.10 | 2.55 |
| $Cr_2O_3$ | 0.04 | 0.06 | 0.08 |
| *FeO | 8.31 | 7.84 | 7.90 |
| MnO | 0.25 | 0.29 | 0.24 |
| MgO | 14.18 | 14.04 | 14.30 |
| CaO | 20.57 | 20.58 | 21.01 |
| $Na_2O$ | 0.52 | 0.60 | 0.05 |
| $K_2O$ | 0 | 0 | 0 |
| Total | 96.55 | 99.88 | 98.68 |
| Number of Ions based on 6 Oxygen | | | |
| Si | 1.92 | 1.93 | 1.95 |
| Ti | 0.02 | 0.02 | 0.01 |
| Al | 0.16 | 0.14 | 0.11 |
| Cr | 0.00 | 0.00 | 0.00 |
| Fe | 0.26 | 0.25 | 0.25 |
| Mn | 0.01 | 0.01 | 0.01 |
| Mg | 0.78 | 0.79 | 0.80 |
| Ca | 0.82 | 0.83 | 0.85 |
| Na | 0.04 | 0.04 | 0.00 |
| K | 0.00 | 0.00 | 0.00 |
| Total | 4.00 | 4.00 | 3.98 |

**Amphiboles**

Amphiboles were found and analyzed using the electron microprobe on two radial dikes (samples IC-SPD4 and SR-8) and two cognate xenoliths (samples IC-7 and IC-14a). Varieties of amphibole identified to exist within the West Spanish Peak intrusive complex include kaersutite and pargasite. Kaersutite is a titanium rich amphibole with slightly lower levels of magnesium, while pargasite is a slightly more magnesium rich amphibole and contains less titanium.

***Radial Dikes***

Analyses of two radial dike samples (samples IC-SPD4 and SR-8b) show that the they contain a type of amphibole called kaersutite, which is a titanium rich amphibole. Weight percent oxides for titanium in these radial dikes range from 4.15 – 4.91 percent, while weight percent oxides for magnesium range from 12.53 – 13.38 percent. It is important to note that although all amphiboles found within this dike are kaersutitic, there have been analyses performed in which radial dikes can also display pargasitic amphibole, notably by Contreras (2014).

**Table 3.4:** Amphibole electron probe oxide data for radial dikes surrounding West Spanish Peak (samples IC-SPD4 and SR-8b).

| **Sample:** | **IC-SPD4** | | | **SR-8b** | | |
|---|---|---|---|---|---|---|
| | Kaersutite 1 | Kaersutite 2 | Kaersutite 3 | Kaersutite 1 | Kaersutite 2 | Kaersutite 3 |
| $SiO_2$ | 38.42 | 40.48 | 38.78 | 39.28 | 39.44 | 39.98 |
| $TiO_2$ | 4.15 | 4.43 | 4.28 | 4.81 | 4.91 | 4.82 |
| $Al_2O_3$ | 11.26 | 11.57 | 10.95 | 12.44 | 12.80 | 11.58 |
| $Cr_2O_3$ | 0.00 | 0.00 | 0.00 | 0.00 | 0.05 | 0.00 |
| *FeO | 11.31 | 11.09 | 10.86 | 10.91 | 11.27 | 10.70 |
| MnO | 0.24 | 0.16 | 0.24 | 0.15 | 0.13 | 0.19 |
| MgO | 12.77 | 12.98 | 13.38 | 13.06 | 12.53 | 13.29 |
| CaO | 11.14 | 11.16 | 11.22 | 11.36 | 11.36 | 11.31 |
| $Na_2O$ | 2.50 | 2.53 | 2.57 | 2.47 | 2.49 | 2.53 |
| $K_2O$ | 1.03 | 1.04 | 1.05 | 0.95 | 0.97 | 0.97 |
| Total | 92.85 | 95.48 | 93.35 | 95.45 | 95.98 | 95.40 |
| Number of Ions based on 24 Oxygen | | | | | | |
| Si | 6.29 | 6.40 | 6.30 | 6.22 | 6.21 | 6.32 |
| Ti | 0.51 | 0.53 | 0.52 | 0.57 | 0.58 | 0.58 |
| Al | 2.17 | 2.15 | 2.10 | 2.32 | 2.38 | 2.19 |
| Cr | 0 | 0 | 0 | 0 | 0.01 | 0 |
| Fe | 1.55 | 1.47 | 1.48 | 1.44 | 1.48 | 1.42 |
| Mn | 0.03 | 0.02 | 0.03 | 0.02 | 0.02 | 0.03 |
| Mg | 3.11 | 3.06 | 3.24 | 3.08 | 2.94 | 3.13 |
| Ca | 1.95 | 1.89 | 1.95 | 1.93 | 1.92 | 1.92 |
| Na | 0.79 | 0.78 | 0.81 | 0.76 | 0.76 | 0.78 |
| K | 0.22 | 0.21 | 0.22 | 0.19 | 0.20 | 0.20 |
| Total | 16.62 | 16.50 | 16.64 | 16.53 | 16.49 | 16.51 |

***Cognate Xenoliths***

The analyses shows that these cognate xenoliths (samples IC-7 and IC-14a) contain both kaersutite and pargasite. The first cognate xenolith (sample IC-7) displays both varieties of amphibole simultaneously, but even though both are present this sample contains kaersutite, with only one pargasite grain having been analyzed. The second cognate xenolith on the otherhand contains exclusively pargasite amphibole. Weight percent oxides for titanium found in kaersututic grains within

cognate xenoliths range from 4.16 – 4.45 percent, and for magnesium range from 12.41 - 12.71 percent. While pargasitic grains within cognate xenoliths have weight percent oxides for titanium ranging from 3.5 – 4.01 percent, and for magnesium ranging from 12.49 - 13.47 percent.

**Table 3.5:** Amphibole electron probe data for a cognate xenoliths found within a radial dike (samples IC-7 and IC-14a).

| **Sample:** | **IC-7** | | | | **IC-14a** | | |
|---|---|---|---|---|---|---|---|
| | Kaersutite 1 | Kaersutite 2 | Kaersutite 3 | Pargasite 1 | Pargasite 1 | Pargasite 2 | Pargasite 3 |
| $SiO_2$ | 38.23 | 39.37 | 38.08 | 39.34 | 41.33 | 40.81 | 40.26 |
| $TiO_2$ | 4.45 | 4.43 | 4.16 | 3.80 | 4.00 | 3.50 | 4.01 |
| $Al_2O_3$ | 11.65 | 11.65 | 11.48 | 11.10 | 11.85 | 11.88 | 11.86 |
| $Cr_2O_3$ | 0.03 | 0.03 | 0.00 | 0.00 | 0.22 | 0.27 | 0.26 |
| *FeO | 11.62 | 11.45 | 11.60 | 12.60 | 11.51 | 11.55 | 10.37 |
| MnO | 0.23 | 0.18 | 0.21 | 0.25 | 0.14 | 0.22 | 0.14 |
| MgO | 12.41 | 12.71 | 12.45 | 12.49 | 13.14 | 13.05 | 13.47 |
| CaO | 11.09 | 10.99 | 11.12 | 10.90 | 11.10 | 11.13 | 11.29 |
| $Na_2O$ | 2.43 | 2.43 | 2.44 | 2.17 | 2.62 | 2.61 | 2.63 |
| $K_2O$ | 1.21 | 1.19 | 1.17 | 1.12 | 0.81 | 0.92 | 0.80 |
| Total | 93.39 | 94.46 | 92.73 | 93.79 | 96.73 | 95.97 | 95.11 |
| Number of Ions based on 24 Oxygen | | | | | | | |
| Si | 6.23 | 6.32 | 6.25 | 6.38 | 6.43 | 6.42 | 6.36 |
| Ti | 0.55 | 0.54 | 0.51 | 0.46 | 0.47 | 0.41 | 0.48 |
| Al | 2.24 | 2.20 | 2.22 | 2.12 | 2.15 | 2.20 | 2.21 |
| Cr | 0.00 | 0.00 | 0.00 | 0.00 | 0.03 | 0.03 | 0.03 |
| Fe | 1.58 | 1.54 | 1.59 | 1.71 | 1.50 | 1.52 | 1.37 |
| Mn | 0.03 | 0.02 | 0.03 | 0.03 | 0.02 | 0.03 | 0.02 |
| Mg | 3.02 | 3.04 | 3.05 | 3.02 | 3.05 | 3.06 | 3.17 |
| Ca | 1.94 | 1.89 | 1.96 | 1.90 | 1.85 | 1.88 | 1.91 |
| Na | 0.77 | 0.76 | 0.78 | 0.68 | 0.79 | 0.80 | 0.81 |
| K | 0.25 | 0.24 | 0.25 | 0.23 | 0.16 | 0.19 | 0.16 |
| Total | 16.61 | 16.55 | 16.63 | 16.55 | 16.47 | 16.54 | 16.53 |

## Feldspars

Plagioclase feldspars were found in all samples in this study with the exception of one cognate xenolith (sample IC-14a). In addition, the West Spanish Peak stock (sample IC-16) is the only sample to contain alkali feldspar included into this study. Only the feldspars in the West Spanish Peak stock (sample IC-16) were analyzed using the electron microprobe in this study because feldspars have been examined by previous studies, notably by Contreras (2014), to examine the variety of feldpsars present in the Spanish Peaks intrusive suite. The results of Contreras (2014) are compared alongside the results from electron microprobe analysis from this study on sample IC-16 (Figure 3.2).

### *West Spanish Peak*

Of the three feldspars from the West Spanish Peak stock (sample IC-16) analyzed using the electron microprobe, two are plagioclase feldspars and one is an alkali feldspar. The plagioclase feldspars vary from 6.78 - 7.89 percent in sodium content, while the alkali feldspar has a sodium content of 1.46 percent. The plagioclase feldspars range in calcium content from 4.08 – 7.61 percent, and the alkali feldspar having almost no calcium with 0.01 percent present. The plagioclase feldspar are nearly devoid of potassium, ranging from 0.39 – 0.55 percent, while the alkali feldspar is 14.92 percent potassium.

The plagioclase feldspars present in the West Spanish Peak stock are a sodic plagioclase, oligioclase, as well as a relatively more calcic, transitional plagioclase, andesine. The alkali feldspar phase present in this sample is orthoclase. The first plagioclase plots on the feldspar ternary diagram at $Ab_{88}An_{22}$, placing it in the Oligioclase phase range ($Ab_{70\text{-}90}An_{10\text{-}30}$). The second plagioclase plots on the feldspar ternary diagram at $Ab_{62}An_{38}$, placing it in the Andesine phase range ($Ab_{50\text{-}70}An_{30\text{-}50}$). The alkali feldspar plots on the ternary diagram at $Or_{87}Ab_{13}$ placing it in the orthoclase phase range ($Or_{70\text{-}90}Ab_{10\text{-}30}$).

**Figure 3.2:** Plot of feldpsar variation between West Spanish Peak stock, a radial dike hosting xenoliths, and cognate xenolith samples. Cognate xenoliths and host radial dike plagioclase values are reported from Contreras (2014). Axes are in Mol. Precentage.

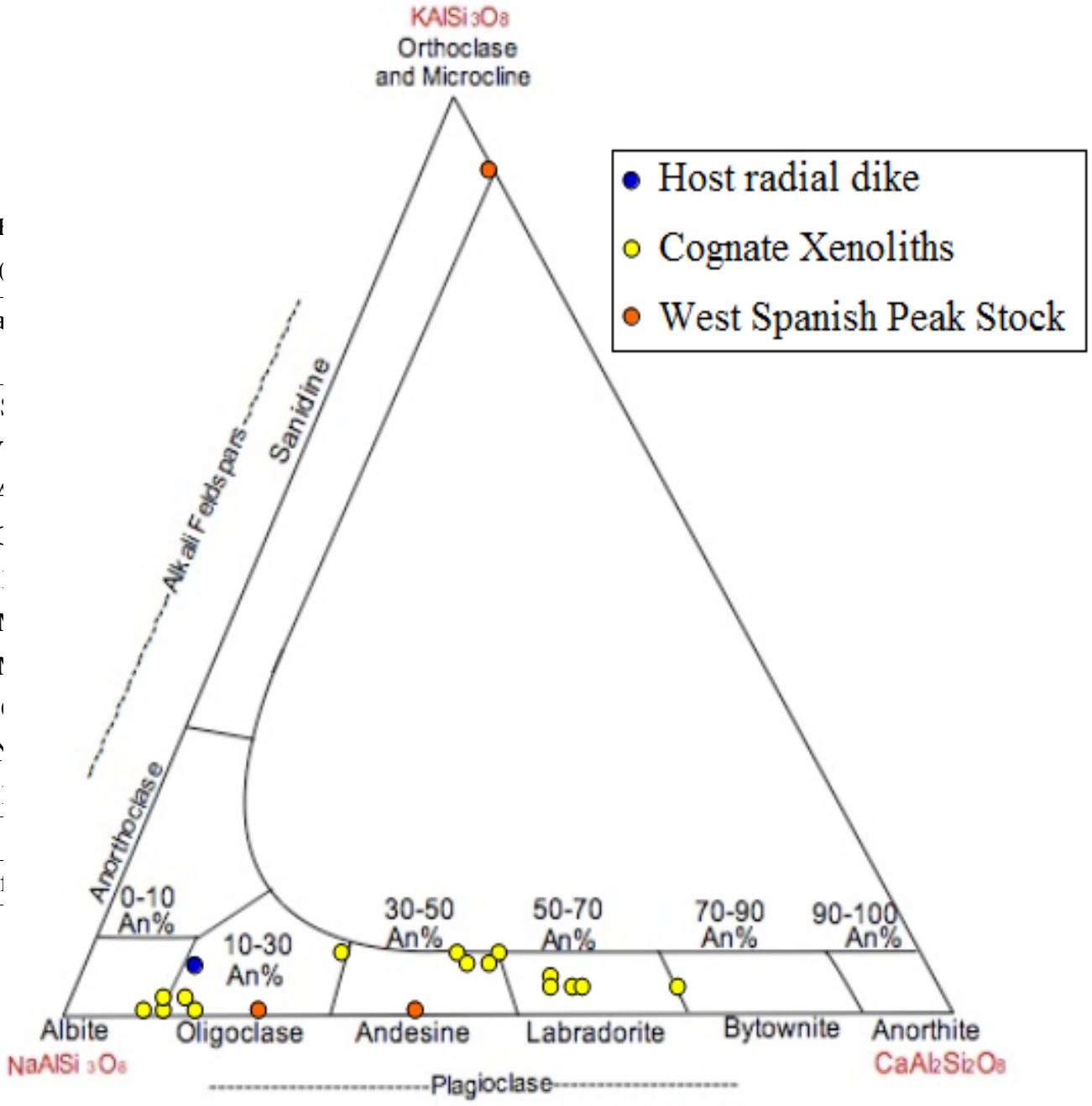


**Table 3.6:** I

Peak stock (

| Sa | | | |
|---|---|---|---|
| | | | |
| Total | | | |
| Number o | | | |
| Mn | 0.00 | 0.00 | 0.00 |
| Mg | 0.00 | 0.00 | 0.00 |
| Ca | 0.22 | 0.40 | 0.00 |
| Na | 0.78 | 0.64 | 0.14 |
| K | 0.03 | 0.03 | 0.96 |

| | | | |
|---|---|---|---|
| Total | 5.02 | 5.03 | 5.08 |

**Biotite**

Biotite was probed using the electron microprobe on the West Spanish Peak stock (sample IC-16) in this study. The West Spanish Peak stock was the only sample probed in this study because it was the only sample with biotite present. Analytical results of microprobe analysis on biotite can be found in Table 3.7.

***West Spanish Peak***

The biotite present in the West Spanish Peak stock (sample IC-16) has roughly twice the amount of magnesium composing in comparison to iron. Magnesium content in the biotites analyzed by the elctron microprobe range from 14.86 -15.86 percent. Iron content on the other hand ranges from 13.37-14.55 percent. This means that in the solid solution series between annite an phlogopite, the biotite present in sample IC-16 lies at roughly $An_{33}Phl_{67}$, meaning the biotite phase present best represents a ferrous-phlogopite.

**Table 3.7:** Biotite electron probe oxide data for the West Spanish Peak stock (sample IC-16).

| **Sample:** | **IC-16** | |
|---|---|---|
| | Biotite 1 | Biotite 2 |
| $SiO_2$ | 37.07 | 37.04 |
| $TiO_2$ | 5.73 | 5.22 |
| $Al_2O_3$ | 12.34 | 12.22 |
| $Cr_2O_3$ | 0.00 | 0.00 |
| FeO | 13.37 | 14.55 |
| MnO | 0.04 | 0.03 |
| MgO | 15.86 | 14.86 |
| CaO | 0.01 | 0.04 |
| $Na_2O$ | 0.40 | 0.20 |
| $K_2O$ | 9.81 | 9.63 |
| Total | 95.66 | 94.31 |
| Number of Ions based on 12 Oxygen | | |
| Si | 3.05 | 3.08 |
| Ti | 0.33 | 0.33 |
| Al | 1.20 | 1.20 |
| Cr | 0 | 0 |
| Fe | 0.92 | 1.01 |
| Mn | 0.00 | 0.00 |
| Mg | 1.94 | 1.84 |
| Ca | 0.00 | 0.00 |
| Na | 0.06 | 0.03 |
| K | 1.03 | 1.02 |

| | | |
|---|---|---|
| Total | 8.55 | 8.52 |

**Oxides**

Opaque minerals, which are mostly oxide minerals, were identified in all seven samples that were analyzed under the electron microprobe in this study. Samples analyzed by the electron microprobe included into this study are: one plutonic stock (sample IC-16), three radial dikes (samples SR-7, SR-8b and IC-SPD4), two cognate xenoliths (samples IC-7 and IC-14a) were and one miarolitic cavity (sample TJ-2a). The main purpose of identifying the oxide phases present is to resolve an apparent dichotmy that exists between illmenite and titanomagnetite in the West Spanish Peak intrusive suite. Analytical results from the electron microprobe are displayed in Tables 3.8 through 3.11.

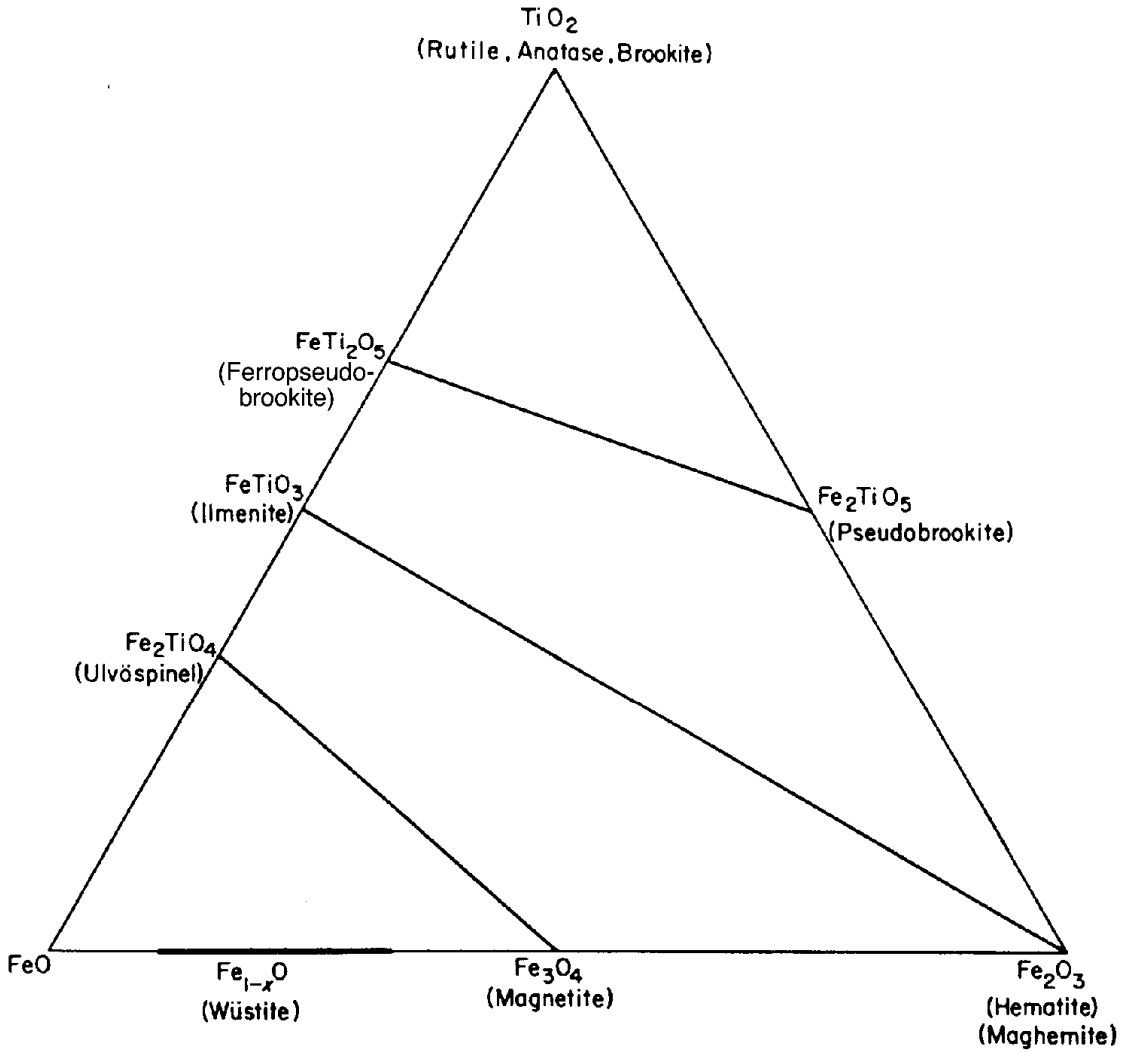


**Figure 3.3:** Ternary diagram between FeO-Fe2O3-TiO2 end members with solid solution lines shown. The abundance of ilmenite and titanomagnetite (ulvospinel) is present between samples analyzed.

***West Spanish Peak***

Three different varieties of oxide minerals were identified within the West Spanish Peak stock (sample IC-16) including: ilmenite, titanomagnetite, and hematite. Ilmenite weight percent oxides for iron range from 46.99 - 53.02 percent, and for titantium, range from 44.59 – 50.30 percent. For titanomagnetites, weight percent oxides for iron ranges between 79.11 – 88.22 percent, and for titanium ranges from 4.86 – 19.36 percent. The hematite samples found in the plutonic stock contain almost entirely all iron, with weight percent oxides for iron ranging from 95.18 – 98.70 percent. The presence of both ilmenite and titatnomagnetite in the West Spanish Peak stock is interesting because ilmenite typically forms in an alkaline rich environment, while titanomagnetites form in a calc-alkaline environment.

**Table 3.8:** Opaque minerals electron probe oxide data for the West Spanish Peak stock (sample IC-16).

| **Sample:** | **IC-16** | | | | | | |
|---|---|---|---|---|---|---|---|
| | Ilmenite 1 | Ilmenite 2 | Titanomagnetite 1 | Titanomagnetite 2 | Hematite 1 | Hematite 2 | Hematite 3 |
| $SiO_2$ | 0.00 | 0.00 | 5.03 | 0.03 | 3.00 | 0.03 | 0.04 |
| $TiO_2$ | 44.59 | 50.39 | 4.54 | 19.36 | 0.00 | 0.56 | 2.21 |
| $Al_2O_3$ | 0.04 | 0.01 | 1.04 | 0.45 | 0.35 | 0.30 | 0.29 |
| $Cr_2O_3$ | 0.04 | 0.04 | 0.31 | 0.18 | 0.01 | 0.29 | 0.22 |
| *FeO | 53.02 | 46.99 | 82.36 | 79.11 | 80.73 | 95.82 | 95.18 |
| MnO | 1.86 | 2.43 | 0.06 | 0.84 | 0.14 | 0.09 | 0.19 |
| MgO | 0.03 | 0.04 | 0.01 | 0.02 | 0.05 | 0.00 | 0.00 |
| Total | 99.59 | 99.90 | 93.35 | 99.99 | 84.28 | 97.08 | 98.13 |
| Number of Ions based on: | 3 Oxygen | | 4 Oxygen | | 3 Oxygen | | |
| Si | 0.00 | 0.00 | 0.00 | 0.00 | 0.12 | 0.00 | 0.00 |
| Ti | 0.90 | 0.97 | 0.16 | 0.60 | 0.00 | 0.01 | 0.06 |
| Al | 0.00 | 0.00 | 0.06 | 0.02 | 0.02 | 0.01 | 0.01 |
| Cr | 0.00 | 0.00 | 0.01 | 0.01 | 0.00 | 0.01 | 0.01 |
| Fe | 1.18 | 1.01 | 3.13 | 2.73 | 2.73 | 2.93 | 2.85 |
| Mn | 0.04 | 0.05 | 0.00 | 0.03 | 0.01 | 0.00 | 0.01 |
| Mg | 0.00 | 0.00 | 0.00 | 0.00 | 0.00 | 0.00 | 0.00 |
| Total | 2.11 | 2.03 | 3.58 | 3.39 | 2.87 | 2.97 | 2.93 |

***Radial Dikes***

The different varieties of oxide minerals were identified within the radial dikes around West Spanish Peak (samples SR-7, IC-SPD4, and SR-8b) include ilmenite, and titanomagnetite. Ilmenite weight percent oxides for iron range from 44.16 – 58.48 percent, and for titantium, range from 32.45 –

43.56 percent. For titanomagnetites, weight percent oxides for iron ranges between 64.69 – 88.33 percent, and for titanium ranges from 6.26 – 22.61 percent. Of the three dikes samples, two (samples SR-7 and SR-8b) contained both ilmenite and titanomagnetite, both displaying more titanomagnetite than ilmenite, while one radial dike sample (sample IC-SPD4) contained exclusively titanomagnetites. The presence of both ilmenite and titanomagnetite in the radial dikes is also interesting to note because again ilmenite forms in under alkaline conditions while titanomagnetite is associated with calc-alkaline conditions.

**Table 3.9:** Opaque minerals electron probe oxide data for radial dikes (samples SR-7, IC-SPD4, and SR-8b).

| **Sample:** | **SR-7** | **IC-SPD4** | **SR-8b** |
|---|---|---|---|

| | Ilmenite 1 | Titanomagnetie 1 | Titanomagnetie 2 | Titanomagnetie 3 | Titanomagnetie 4 | Titanomagnetite 1 | Titanomagnetie 2 | Titanomagnetie 3 | Titanomagnetie 4 | Titanomagnetie 5 | Ilmenite 1 | Ilmenite 2 | Titanomagnetite 1 | Titanomagnetite 1 | Titanomagnetite 2 |
|---|---|---|---|---|---|---|---|---|---|---|---|---|---|---|---|
| $SiO_2$ | 0.00 | 0.71 | 0.94 | 0.95 | 1.18 | 3.04 | 0.77 | 0.06 | 0.09 | 0.09 | 0.21 | 0.47 | 0.17 | 0.06 | 0.09 |
| $TiO_2$ | 33.9 | 11.1 | 12.6 | 8.31 | 13.7 | 12.8 | 8.99 | 8.60 | 13.8 | 12.5 | 32.5 | 43.6 | 22.6 | 12.4 | 6.26 |
| $Al_2O_3$ | 0.69 | 2.48 | 3.50 | 2.28 | 2.26 | 3.72 | 4.30 | 3.62 | 2.56 | 3.30 | 0.24 | 1.46 | 0.04 | 3.01 | 0.51 |
| $Cr_2O_3$ | 0.00 | 0.12 | 0.71 | 0.08 | 0.45 | 0.06 | 1.02 | 0.01 | 0.09 | 1.23 | 0.02 | 0.03 | 0.02 | 0.07 | 0.11 |
| *FeO | 50.9 | 66.5 | 64.7 | 68.9 | 68.4 | 68.8 | 78.2 | 79.6 | 76.5 | 76.0 | 58.4 | 44.2 | 67.7 | 77.6 | 88.3 |
| MnO | 1.64 | 0.44 | 0.29 | 0.22 | 0.23 | 0.29 | 0.26 | 0.50 | 0.29 | 0.34 | 1.85 | 0.24 | 5.48 | 2.17 | 1.23 |
| MgO | 2.24 | 0.00 | 0.18 | 0.08 | 0.01 | 0.74 | 0.33 | 1.22 | 0.01 | 0.01 | 0.02 | 0.24 | 0.00 | 0.03 | 0.02 |
| Total | 89.39 | 81.34 | 82.92 | 80.80 | 86.21 | 89.45 | 93.83 | 93.66 | 93.30 | 93.50 | 93.24 | 90.16 | 96.00 | 95.32 | 96.54 |
| Number of Ions | 3 Oxygen | 4 Oxygen | | | | 4 Oxygen | | | | | 3 Oxygen | | 4 Oxygen | | |
| Si | 0.00 | 0.04 | 0.05 | 0.05 | 0.06 | 0.13 | 0.03 | 0.00 | 0.00 | 0.00 | 0.00 | 0.01 | 0.01 | 0.00 | 0.00 |
| Ti | 0.77 | 0.43 | 0.46 | 0.33 | 0.49 | 0.42 | 0.30 | 0.29 | 0.46 | 0.42 | 0.73 | 0.92 | 0.71 | 0.41 | 0.22 |
| Al | 0.02 | 0.15 | 0.20 | 0.14 | 0.13 | 0.19 | 0.23 | 0.19 | 0.13 | 0.17 | 0.01 | 0.05 | 0.00 | 0.16 | 0.03 |
| Cr | 0.00 | 0.01 | 0.03 | 0.00 | 0.02 | 0.00 | 0.04 | 0.00 | 0.00 | 0.05 | 0.00 | 0.00 | 0.00 | 0.00 | 0.00 |
| Fe | 1.28 | 2.83 | 2.62 | 3.01 | 2.70 | 2.53 | 2.91 | 3.02 | 2.85 | 2.82 | 1.46 | 1.04 | 2.37 | 2.85 | 3.45 |
| Mn | 0.04 | 0.02 | 0.01 | 0.01 | 0.01 | 0.01 | 0.01 | 0.02 | 0.01 | 0.01 | 0.05 | 0.00 | 0.19 | 0.08 | 0.05 |
| Mg | 0.10 | 0.00 | 0.01 | 0.01 | 0.00 | 0.05 | 0.02 | 0.08 | 0.00 | 0.00 | 0.00 | 0.01 | 0.00 | 0.00 | 0.00 |

| | | | | | | | | | | | | | | | |
|---|---|---|---|---|---|---|---|---|---|---|---|---|---|---|---|
| Total | 2.22 | 3.46 | 3.38 | 3.55 | 3.39 | 3.35 | 3.53 | 3.61 | 3.47 | 3.47 | 2.26 | 2.04 | 3.28 | 3.51 | 3.76 |

***Cognate Xenoliths***

Oxide minerals identified within cognate xenoliths (samples IC-7 and IC-14a) found within the radial dikes around West Spanish Peak include exclusively titanomagnetite. For titanomagnetites in these samples, weight percent oxides for iron ranges between 76.15 – 84.98 percent, and for titanium ranges from 3.40 – 11.34 percent. Of the two xenolith samples, the second xenolith (sample IC-14a) contains an apparent enrichment in chromium in comparison to the first xenolith (sample IC-7), as well as in comparison to any other sample included in this study. The fact that only titanomagnetite is observed in the cognate xenoliths indicates that the source of the xenolith samples is representative of a calc-alkaline environment.

**Table 3.10:** Opaque minerals electron probe oxide data for cognate xenoliths (samples IC-7 and IC-14a).

| **Sample:** | **IC-7** | | | | **IC-14a** | | | | |
|---|---|---|---|---|---|---|---|---|---|
| | Titanomagnetite 1 | Titanomagnetie 2 | Titanomagnetie 3 | Titanomagnetie 4 | Titanomagnetite 1 | Titanomagnetie 2 | Titanomagnetie 3 | Titanomagnetie 4 | Titanomagnetie 5 |
| $SiO_2$ | 0.15 | 0.78 | 0.63 | 0.10 | 0.58 | 0.04 | 3.67 | 0.30 | 0.38 |
| $TiO_2$ | 8.53 | 11.34 | 7.22 | 9.43 | 7.99 | 8.44 | 3.40 | 6.87 | 7.45 |
| $Al_2O_3$ | 3.40 | 3.55 | 1.711 | 4.67 | 1.0163 | 4.89 | 0.4168 | 4.51 | 4.29 |
| $Cr_2O_3$ | 0.13 | 0.19 | 0.01 | 0.04 | 2.46 | 2.93 | 2.44 | 2.77 | 1.77 |
| *FeO | 82.39 | 77.05 | 84.98 | 81.44 | 80.18 | 76.15 | 80.75 | 77.85 | 78.81 |
| MnO | 0.11 | 0.08 | 0.14 | 0.18 | 0.69 | 1.56 | 0.07 | 0.34 | 0.29 |
| MgO | 0.02 | 0.12 | 0.02 | 0.05 | 0.06 | 0.11 | 0.02 | 0.07 | 0.10 |
| Total | 94.74 | 93.10 | 94.71 | 95.91 | 92.98 | 94.11 | 90.78 | 92.70 | 93.09 |
| Number of Ions based on: | 4 Oxygen | | | | 4 Oxygen | | | | |
| Si | 0.01 | 0.04 | 0.03 | 0.00 | 0.03 | 0.00 | 0.18 | 0.01 | 0.02 |
| Ti | 0.29 | 0.38 | 0.25 | 0.31 | 0.28 | 0.28 | 0.12 | 0.24 | 0.26 |
| Al | 0.18 | 0.19 | 0.09 | 0.24 | 0.06 | 0.26 | 0.02 | 0.24 | 0.23 |
| Cr | 0.00 | 0.01 | 0.00 | 0.00 | 0.09 | 0.10 | 0.09 | 0.10 | 0.06 |
| Fe | 3.12 | 2.87 | 3.29 | 2.99 | 3.13 | 2.83 | 3.23 | 2.97 | 3.00 |
| Mn | 0.00 | 0.00 | 0.01 | 0.01 | 0.03 | 0.00 | 0.00 | 0.01 | 0.01 |

| | | | | | | | | | |
|---|---|---|---|---|---|---|---|---|---|
| Mg | 0.00 | 0.01 | 0.00 | 0.00 | 0.01 | 0.01 | 0.00 | 0.01 | 0.01 |
| Total | 3.61 | 3.49 | 3.67 | 3.57 | 3.62 | 3.54 | 3.65 | 3.58 | 3.58 |

***Miarolitic Cavity***

The only oxide phase probed using the electron microprobe on a miarolitic cavity (sample TJ-2a) was a hematite grain found associated with a suite of sulfides within the opaque portion of the cavity. Hematite in this sample is made of almost entirely iron, with weight percent oxides for iron being reported at ~98% of this mineral grain. Two forms of hematite were found within this sample, both botryoidal and platty hematite were found along side pyrite, chalcopyrite, and a cobalt sulfide mineral, all contained within a barite mass. The hematite is on the edge of inner edge of this barite mass, often containing sulfide phases within the hematite grains.

**Table 3.11:** Opaque minerals electron probe oxide data for a miarolitic cavity (sample TJ-2a).

| **Sample** | **TJ-2a** |
|---|---|
| | Hematite 1 |
| $SiO_2$ | 1.15 |
| $TiO_2$ | 0.07 |
| $Al_2O_3$ | 0.06 |
| $Cr_2O_3$ | 0.00 |
| *FeO | 82.17 |
| MnO | 0.00 |
| MgO | 0.03 |
| Total | 83.48 |
| Number of Ions based on: | 3 Oxygens |
| Si | 0.05 |
| Ti | 0.00 |
| Al | 0.00 |
| Cr | 0.00 |
| Fe | 2.89 |
| Mn | 0.00 |
| Mg | 0.00 |
| Total | 2.95 |

## Sulfides

Sulfide major element analysis was conducted on the West Spanish Peak stock (sample IC-16) and one miarolitic cavity sample (sample TJ-2a) using the electron microprode for this study. The miarolitic cavity investigated was chosen because of the presence of a cobalt sulfide that was identified and described by Johnson (2014) in sample TJ-2a. The purpose of conducting this study was to identify the exact chemical composition of this sulfide, and to determine if sulfides within the miarolitic cavity bear any resemblance to sulfides within the stock of West Spanish Peak. In doing so, a relationship exists between the plutonic stock and miarolitic cavities found within the radial dikes surrounding the stock. Analytical results of trace elements found within these samples are displayed in Table 3.12 and 3.13.

### *West Spanish Peak*

The only sulfide phase present in the West Spanish Peak stock (sample IC-16) is pyrite. Interestingly, this pyrite grain was found entirely enclosed by an ilmenite grain. The iron content of this pyrite is ~58 percent while the sulfur content of this grain is ~40 percent.

**Table 3.12:** Sulfide electron probe element data from the West Spanish Peak stock (sample IC-16).

| **Sample** | **IC-16** |
|---|---|
| | Pyrite 1 |
| S | 40.22 |
| Fe | 57.99 |
| Cu | 0.02 |
| Co | 0.20 |
| Total | 98.40 |

### *Miarolitic Cavity*

Multiple sulfide phases were detected in the miarolitic cavity analyzed (sample TJ-2a), including: pyrite, chalcopyrite, and a cobalt sulfide called carrollite. The iron content of the pyrite present is ~48 percent while the sulfur content of this grain is ~52 percent. Chalcopyrite has iron content ~30 percent, sulfur content of ~35 percent and copper content of ~35 percent. The cobalt sulfide previously reported, but not identified, by Johnson (2014) was finally given a chemical composition due to this electron probe analyses. It has almost no iron (~0 percent) content, ~42 percent

sulfur content, ~20% copper and ~38 percent cobalt content. Thus, revealing that this cobalt sulfide is the mineral carrollite. The two probe analysis conducted on this mineral were done at the center and the rim of the grain respectively to see in the grain was heterogeneous or not. The results from the electron probe came back nearly identical on both the rim and the grain, and it was concluded that the grain is homogenous.

**Table 3.13:** Sulfide electron probe element data from a mirolitic cavity (sample TJ-2a).

| **Sample** | **TJ-2a** | | | | |
|---|---|---|---|---|---|
| | Pyrite 1 | Chalcopyrite 1 | Chalcopyrite 2 | Carrollite 1 | Carrollite 2 |
| S | 52.95 | 34.97 | 35.04 | 41.81 | 41.80 |
| Fe | 47.22 | 30.03 | 29.93 | 0.7020 | 0.7056 |
| Cu | 0.03 | 34.23 | 34.60 | 20.23 | 20.23 |
| Co | 0.07 | 0.05 | 0.04 | 37.28 | 37.65 |
| Total | 100.27 | 99.28 | 99.62 | 100.02 | 100.39 |

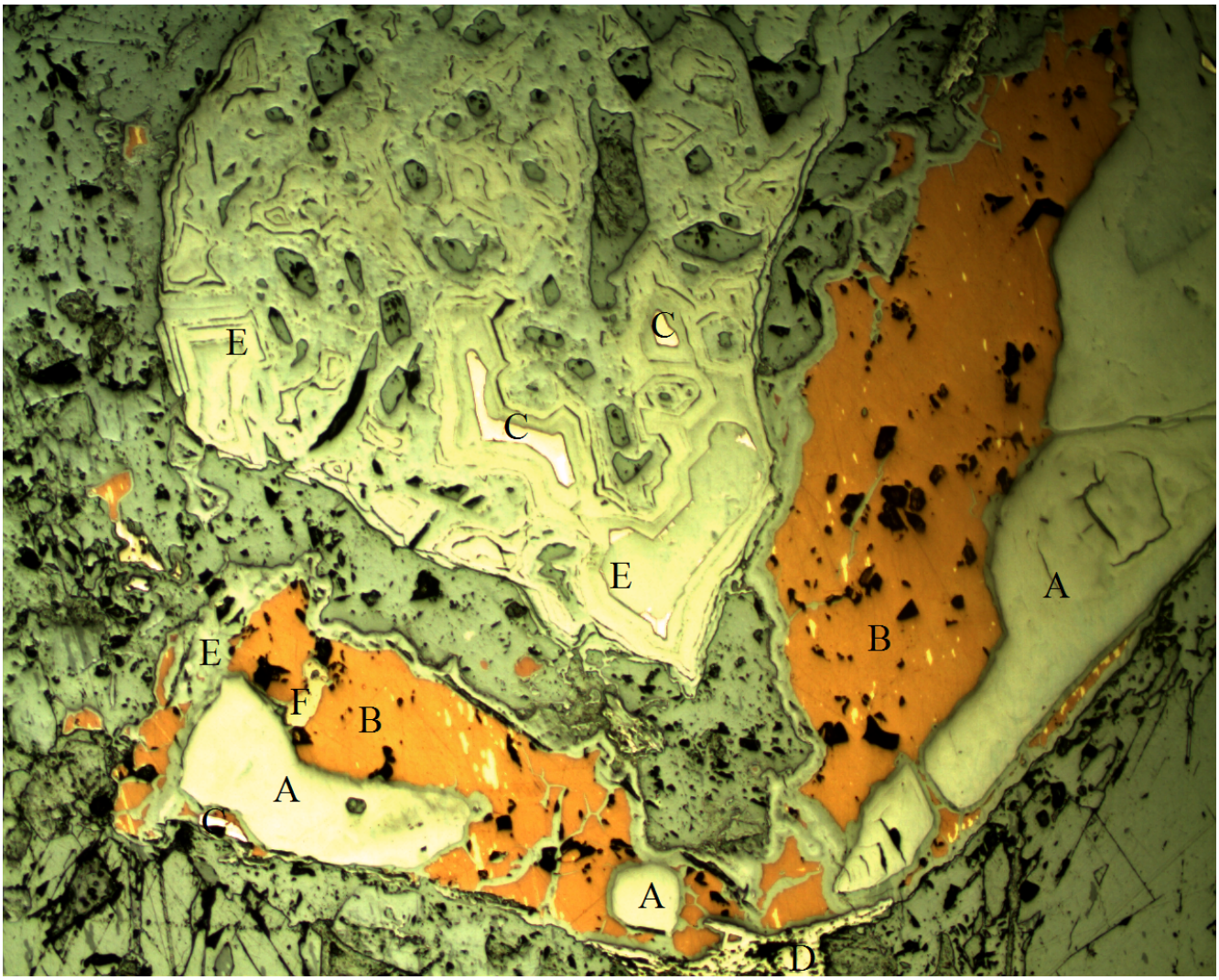


**Figure 3.4:** Sample TJ-2a at 150 times magnification (10x zoom multiplied by 15x ocular) in reflected light. Zoom up of the large opaque mass in which the cobalt sulfide carrollite was discovered. (A) Barite; (B) Chalcopyrite; (C) Pyrite; (D) Platy Hematite; (E) Botryoidal Hematite; (F) Carrollite.

The sample pictured above (sample TJ-2a) is of particular interest because it has been discovered that within the miarolitic cavity of this sample, there is the presence of a cobalt sulfide mineral. This sample was chosen to be incorporated into this study because it was the only sample of a miarolitic cavity discussed by Johnson (2014) to contain the presence of any cobalt sulfide minerals. Using the electron microprobe, it was confirmed that the presence of such a cobalt sulfide exists, and it has been identified as the mineral carrollite, a member of the linnaeite group. This cobalt sulfide appears along side two forms of hematite, pyrite, and chalcopyrite all enclosed within a barite mass. The presence of carrollite in this sample is an indication that metals were mobilized within the groundwater that passed through the radial dikes, depositing metallic sulfides and oxides within the miarolitic cavities.

# Chapter 4

## *Bulk Rock Major and Minor Oxide, Trace Element, and Isotopic Chemistry*

## Introduction

The purpose of this chapter is to present the major and minor weight percent oxides, trace element, rare-earth element (REE), and isotopic data obtained for bulk rock. Samples analyzed for these characteristics in this study include: four radial dikes found around West Spanish Peak, two cognate xenoliths found within radial dikes, as well as two miarolitic cavities. Once analyzed, the data

was compared against data collected in other studies in the Spanish Peaks region, namely by Penn (1994) and Miggins (2002), in order to see if any apparent relationships exist within this suite intrusive igneous features.

**Major and Minor Oxides**

Of the rocks collected for this study, four radial dikes and two cognate xenoliths were analyzed for their major and minor weight percent oxides. Each major and minor oxide is plotted against its $SiO_2$ value, or commonly referred to as Harker variation diagrams, in Figure 4.1. The cognate xenoliths are depleted in $SiO_2$ and, more iron rich, with iron oxides ranging from 11.39 -13.63 weight percent, while the radial dikes only range from 7.64 – 8.24 weight percent. The cognate xenoliths also appear to be enriched in calcium and magnesium in comparison to the radial dikes, ranging from 11.58 – 15.82 and 7.01 – 13.30 weight percent of their respective oxides. Radial dikes in comparison range in calcium oxide from 4.72 – 7.88 weight percent and in magnesium oxide from 3.09 – 4.72 weight percent.

**Table 4.1:** Bulk rock major and minor element oxides for samples analyzed in this study, reported in weight percent oxides. (*All iron reported as Fe2O3.)

| **Sample:** | **SR-7** | **IC-SPD4** | **TJ-7** | **TJ-14** | **IC-7** | **IC-14a** |
|---|---|---|---|---|---|---|
| Type | Radial Dikes | | | | Cognate Xenoliths | |
| $SiO_2$ | 55.70 | 52.60 | 54.40 | 54.90 | 42.30 | 45.90 |
| $Al_2O_3$ | 16.40 | 15.86 | 16.14 | 16.76 | 16.39 | 7.94 |
| *$Fe_2O_3$ | 7.64 | 8.24 | 8.16 | 7.98 | 13.63 | 11.39 |
| MnO | 0.13 | 0.14 | 0.17 | 0.15 | 0.17 | 0.26 |
| MgO | 4.03 | 4.42 | 3.36 | 3.09 | 7.01 | 13.30 |

| | | | | | | |
|---|---|---|---|---|---|---|
| CaO | 4.72 | 7.88 | 5.48 | 5.54 | 11.58 | 15.82 |
| $Na_2O$ | 4.61 | 3.50 | 4.58 | 4.48 | 3.17 | 1.09 |
| $K_2O$ | 2.17 | 2.15 | 1.79 | 1.38 | 0.84 | 0.27 |
| $TiO_2$ | 1.54 | 1.35 | 1.46 | 1.47 | 2.96 | 1.73 |
| $P_2O_5$ | 0.58 | 0.61 | 0.72 | 0.70 | 1.65 | 0.13 |
| Total | 99.77 | 98.18 | 99.26 | 99.14 | 100.40 | 98.71 |

Of the rocks collected from other studies conducted in the same region (Penn (1994) and Miggins (2002)), major and minor oxides were reported for: two samples of the West Spanish Peaks Stock, five radial dikes, and two intrusive sills with intrusion ages which overlaps that of the magmatism associated with West Spanish Peak. These major and minor weight percent oxides are plotted against samples analyzed for this study in Harker variation diagrams in Figure 4.1.The West Spanish Peak stock displays the least amount of iron on average, with iron oxides ranging from 6.31 - 7.06 weight percent, while the radial dikes are also relatively iron poor, wide ranging from 4.86 – 10.84 weight percent. The intrusive sills show the highest iron oxide values on average with a narrow range from 8.15 – 8.46 weight percent.

**Table 4.2:** Bulk rock major and minor element oxides for samples from other studies conducted in the Spanish Peaks area, reported in weight percent oxides. (*All iron reported as Fe2O3.)

| **Sample:** | **sp33** | **98-48** | **sp73** | **sp95** | **sp101** | **98-33** | **98-79** | **98-37** | **98-44b** |
|---|---|---|---|---|---|---|---|---|---|
| Type | WSP Stock | | Radial Dikes | | | | | Intrusive Sills | |
| Source | Penn (1994) | Miggins (2002) | Penn (1994) | Penn (1994) | Penn (1994) | Miggins (2002) | Miggins (2002) | Miggins (2002) | Miggins (2002) |
| $SiO_2$ | 59.10 | 58.50 | 63.00 | 54.40 | 55.90 | 45.00 | 45.90 | 50.80 | 48.70 |
| $Al_2O_3$ | 17.37 | 15.60 | 16.05 | 17.55 | 16.72 | 14.85 | 17.00 | 14.70 | 12.72 |
| *$Fe_2O_3$ | 6.31 | 7.06 | 4.86 | 7.76 | 7.34 | 10.84 | 9.90 | 8.15 | 8.49 |

| | | | | | | | | | |
|---|---|---|---|---|---|---|---|---|---|
| MnO | 0.12 | 0.11 | 0.11 | 0.15 | 0.14 | 0.19 | 0.16 | 0.10 | 0.10 |
| MgO | 2.52 | 2.91 | 2.41 | 4.00 | 4.22 | 6.98 | 4.14 | 4.55 | 6.75 |
| CaO | 4.59 | 4.56 | 3.29 | 6.68 | 7.38 | 9.58 | 9.14 | 7.02 | 5.81 |
| $Na_2O$ | 4.70 | 4.22 | 4.56 | 4.61 | 3.91 | 3.03 | 3.72 | 3.93 | 3.41 |
| $K_2O$ | 3.47 | 3.79 | 4.30 | 2.79 | 2.61 | 1.04 | 1.44 | 1.64 | 1.61 |
| $TiO_2$ | 1.40 | 1.47 | 1.14 | 1.50 | 1.31 | 2.01 | 1.44 | 1.52 | 1.94 |
| $P_2O_5$ | 0.59 | 0.11 | 0.45 | 0.70 | 0.62 | 0.74 | 0.16 | 0.56 | 1.02 |
| Total | 100.12 | 99.02 | 100.12 | 100.15 | 100.15 | 98.86 | 99.41 | 98.52 | 97.13 |

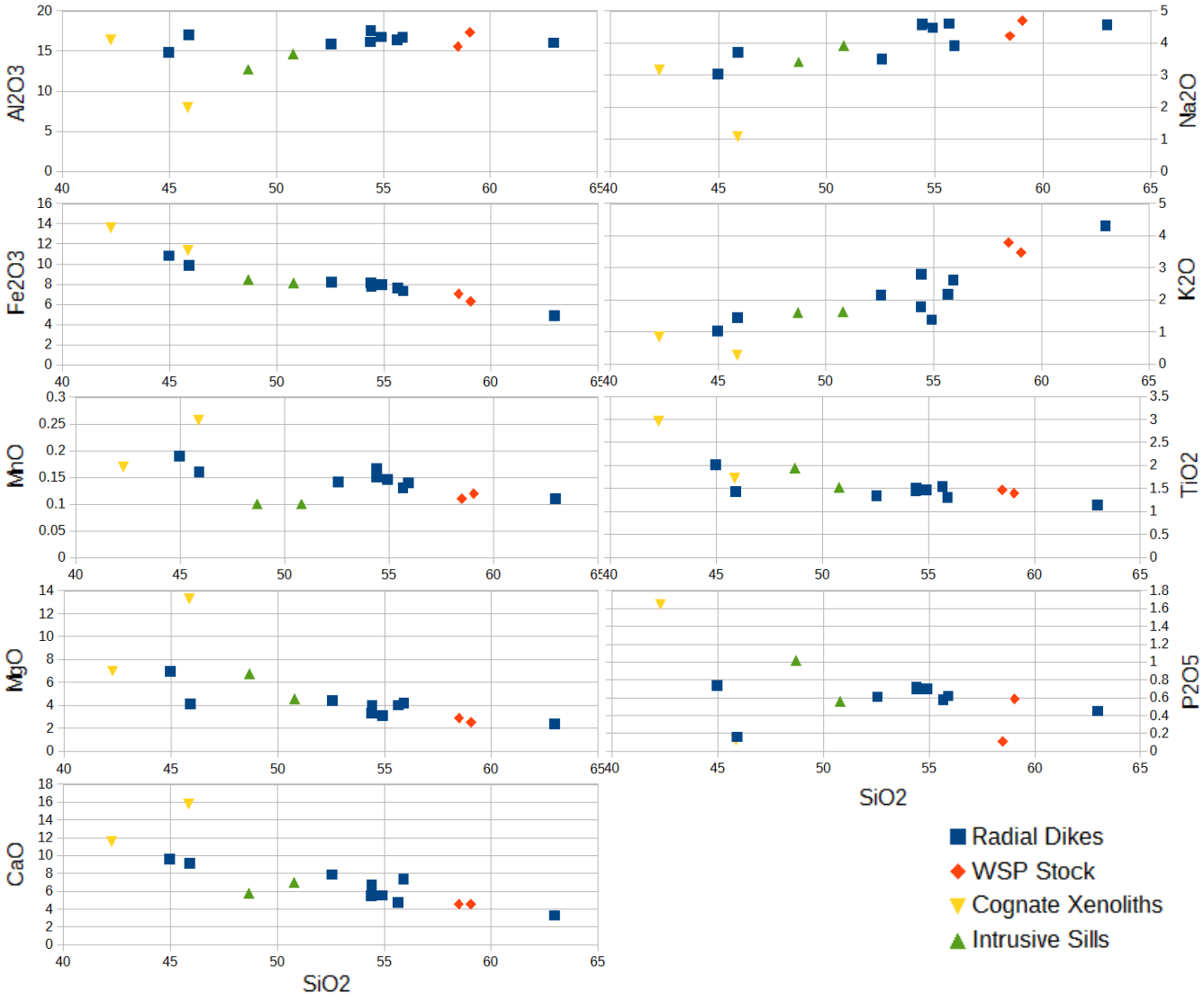
Al2O3
Na2O
Fe2O3
K2O
MnO
TiO2
MgO
P2O5
CaO
SiO2
SiO2
Radial Dikes
WSP Stock
Cognate Xenoliths
Intrusive Sills

**Figure 4.1:** Harker variation diagrams for intrusive rocks in the Spanish Peaks region. Each diagram is SiO2 plotted against a different element oxide, and all values are reported in weight percent oxides. For almost each variation diagram there exists a strong linear relationship between different rocks found within the intrusive suite.

### Trace and Rare-Earth Elements (REEs)

Trace and rare-earth element analyses were also conducted for this study on the same samples tested for major and minor oxides, four radial dikes and two cognate xenoliths, and are reported in parts per million (Figures 4.3 and 4.4). The trace and rare-earth element data is also compared against trace and rare-earth element studies conducted by others in the Spanish Peaks area (Penn (1994), Miggins (2002), and Contreras (2014) on sample IC-16, a sample used for other portions of this study), (Figures 4.5 and 4.6).

**Table 4.3:** Bulk rock trace element data for samples analyzed in this study, reported in parts per million (ppm).

| **Sample:** | **SR-7** | **IC-SPD4** | **TJ-7** | **TJ-14** | **IC-7** | **IC-14a** |
|---|---|---|---|---|---|---|
| Type | Radial Dikes | | | | Cognate Xenoliths | |
| Sc | 11 | 15 | 11 | 10 | 25 | 58 |
| Be | 2 | 2 | 2 | 3 | 3 | 1 |
| V | 152 | 178 | 174 | 169 | 301 | 306 |
| Ba | 1713 | 1161 | 1385 | 1133 | 640 | 151 |
| Sr | 1176 | 1082 | 982 | 1096 | 1379 | 379 |
| Y | 16 | 24 | 21 | 23 | 39 | 24 |
| Zr | 237 | 262 | 270 | 296 | 113 | 90 |
| Cr | 90 | 100 | 40 | 30 | 30 | 630 |
| Co | 28 | 25 | 20 | 20 | 32 | 52 |
| Ni | 60 | 50 | 20 | < 20 | < 20 | 210 |
| Cu | 40 | 40 | 20 | 20 | 50 | < 10 |
| Zn | 110 | 100 | 140 | 130 | 150 | 100 |
| Ga | 21 | 22 | 22 | 22 | 22 | 18 |
| Ge | 1 | 1 | 1 | 2 | 2 | 2 |
| As | < 5 | < 5 | < 5 | < 5 | < 5 | < 5 |
| Rb | 30 | 31 | 30 | 20 | 5 | < 2 |
| Nb | 38 | 37 | 43 | 48 | 37 | 12 |

| | | | | | | |
|---|---|---|---|---|---|---|
| Mo | < 2 | 3 | < 2 | < 2 | < 2 | < 2 |
| Ag | 1.2 | 1.2 | 1.3 | 1.5 | 0.6 | < 0.5 |
| In | < 0.2 | < 0.2 | < 0.2 | < 0.2 | < 0.2 | < 0.2 |
| Sn | 2 | 2 | 2 | 2 | 2 | 1 |
| Sb | < 0.5 | < 0.5 | 0.6 | 0.7 | < 0.5 | 0.6 |
| Cs | < 0.5 | < 0.5 | < 0.5 | < 0.5 | < 0.5 | < 0.5 |

**Table 4.4:** Bulk rock rare-earth element (REE) data for samples from other studies in the Spanish Peaks Region, reported in parts per million (ppm).

| **Sample:** | **SR-7** | **IC-SPD4** | **TJ-7** | **TJ-14** | **IC-7** | **IC-14a** |
|---|---|---|---|---|---|---|
| Type | Radial Dikes | | | | Cognate Xenoliths | |
| La | 47.1 | 54 | 54.4 | 57.5 | 49.8 | 14.8 |
| Ce | 80.9 | 96.1 | 95.3 | 98.2 | 105 | 35 |
| Pr | 9.41 | 11.5 | 11.1 | 11.4 | 14.5 | 5.3 |
| Nd | 34 | 42.9 | 40.8 | 41.8 | 62.1 | 25.4 |
| Sm | 5.8 | 7.5 | 7 | 7.1 | 12.4 | 6.1 |
| Eu | 1.83 | 2.06 | 1.97 | 1.92 | 3.56 | 1.84 |
| Gd | 5.2 | 6.6 | 6.3 | 6.1 | 12.2 | 6.7 |
| Tb | 0.7 | 0.9 | 0.9 | 0.8 | 1.6 | 0.9 |
| Dy | 3.7 | 5.0 | 4.6 | 4.6 | 8.6 | 5.3 |
| Ho | 0.7 | 1 | 0.8 | 0.9 | 1.6 | 1 |
| Er | 1.9 | 2.9 | 2.5 | 2.5 | 4.1 | 2.7 |
| Tm | 0.26 | 0.41 | 0.37 | 0.36 | 0.55 | 0.38 |
| Yb | 1.4 | 2.6 | 2.2 | 2.2 | 3.3 | 2.1 |
| Lu | 0.20 | 0.38 | 0.31 | 0.32 | 0.42 | 0.28 |
| Hf | 5.2 | 5.7 | 5.6 | 6.3 | 3.1 | 2.7 |
| Ta | 2.7 | 2.2 | 3 | 3.1 | 2.1 | 0.7 |
| W | 52 | 49 | 50 | 69 | 30 | 51 |

| | | | | | | |
|---|---|---|---|---|---|---|
| Tl | 0.2 | 0.2 | 0.2 | 0.1 | < 0.1 | < 0.1 |
| Pb | 14 | 10 | 22 | 17 | 11 | 9 |
| Bi | < 0.4 | < 0.4 | < 0.4 | < 0.4 | < 0.4 | < 0.4 |
| Th | 9.7 | 8.6 | 9.9 | 11.1 | 1.6 | 0.8 |
| U | 3 | 2.4 | 2.7 | 3 | 0.5 | 0.2 |

**Table 4.5:** Bulk rock trace element data for samples from other studies in the Spanish Peaks Region (Penn (1994), Miggins (2002) and Contreras (2014)), reported in parts per million (ppm).

| **Sample:** | **sp33** | **98-48** | **IC-16** | **sp58** | **sp95** | **sp101** | **98-33** | **98-79** | **98-37** | **98-44b** |
|---|---|---|---|---|---|---|---|---|---|---|
| Type | WSP Stock | | | Radial Dikes | | | | | Intrusive Sills | |
| Source | Penn (1994) | Miggins (2002) | Contreras (2014) | Penn (1994) | Penn (1994) | Penn (1994) | Miggins (2002) | Miggins (2002) | Miggins (2002) | Miggins (2002) |
| Sc | 7.64 | 9.3 | - | 25.7 | 12.4 | 13.3 | 21.5 | 13.7 | 13.5 | 14.3 |
| Be | - | - | - | - | - | - | - | - | - | - |
| V | - | - | 195 | - | - | - | - | - | - | - |
| Ba | 1160 | 999 | 908 | 1160 | 1490 | 1140 | 644 | 1070 | 1010 | 4720 |
| Sr | 863 | 630 | 706 | 2380 | 1160 | 85 | 850 | 702 | 1090 | 2200 |
| Y | - | - | 22 | - | - | - | - | - | - | - |
| Zr | 305 | 321 | 38 | 198 | 360 | 285 | 189 | 240 | 214 | 345 |
| Cr | 22.6 | 31.4 | 40 | 355 | 43 | 100 | 199 | 4.7 | 139 | 182 |
| Co | - | 18.6 | 25 | - | - | - | 38.6 | 27.7 | 28.3 | 29.3 |
| Ni | 30.2 | 43.1 | 64 | 172 | 30.7 | 38.4 | 125 | 21.1 | 108 | 146 |
| Cu | - | - | 28 | - | - | - | - | - | - | - |
| Zn | - | 103 | 145 | - | - | - | 125 | 117 | 97.1 | 114 |
| Ga | - | - | - | - | - | - | - | - | - | - |
| Ge | - | - | - | - | - | - | - | - | - | - |
| As | - | 2.71 | - | - | - | - | 0.71 | 1.06 | 0.57 | 1.02 |

| | | | | | | | | | | |
|---|---|---|---|---|---|---|---|---|---|---|
| Rb | 84.5 | 111 | 92 | 36 | 51.8 | 51.9 | 15.4 | 23.8 | 25.3 | 27.3 |
| Nb | 88 | - | 58 | 29 | 52 | 47 | - | - | - | - |
| Mo | - | - | - | - | - | - | - | - | - | - |
| Ag | - | - | - | - | - | - | - | - | - | - |
| In | - | - | - | - | - | - | - | - | - | - |
| Sn | - | - | - | - | - | - | - | - | - | - |
| Sb | - | 0.84 | - | - | - | - | 0.10 | 0.10 | 0.17 | 0.10 |
| Cs | - | 3.25 | 2.1 | - | - | - | 0.12 | 0.09 | 0.95 | 0.32 |

**Table 4.6:** Bulk rock rare-earth element (REE) data for samples from other studies in the Spanish Peaks Region (Penn (1994), Miggins (2002) and Contreras (2014)), reported in parts per million (ppm).

| **Sample:** | **sp33** | **98-48** | **IC-16** | **sp58** | **sp95** | **sp101** | **98-33** | **98-79** | **98-37** | **98-44b** |
|---|---|---|---|---|---|---|---|---|---|---|
| Type | WSP Stock | | | Radial Dikes | | | | | Intrusive Sills | |
| Source | Penn (1994) | Miggins (2002) | Contreras (2014) | Penn (1994) | Penn (1994) | Penn (1994) | Miggins (2002) | Miggins (2002) | Miggins (2002) | Miggins (2002) |
| La | 51.2 | 51.2 | 51 | 53.1 | 60.2 | 55.9 | 42.5 | 77.6 | 47.8 | 70.6 |
| Ce | 97.9 | 100 | 98.8 | 113 | 119 | 111 | 78.7 | 141 | 86.3 | 147 |
| Pr | - | - | 11.2 | - | - | - | - | - | - | - |
| Nd | 39.1 | 39.6 | 41 | 51.7 | 51.2 | 47 | 38.5 | 62.4 | 38 | 74 |
| Sm | 7.18 | 7.86 | 8.64 | 8.7 | 8.69 | 8.44 | 7.88 | 10.1 | 7.12 | 12.1 |
| Eu | 2.03 | 1.8 | 2.81 | 2.28 | 2.29 | 2.16 | 2.23 | 2.74 | 1.89 | 2.84 |
| Gd | 5.64 | 5.67 | 8.94 | 6.09 | 7.30 | 6.82 | 6.41 | 7.22 | 5.25 | 8.43 |
| Tb | 0.76 | 0.81 | 0.92 | 0.75 | 0.93 | 0.93 | 0.88 | 1.03 | 0.71 | 0.92 |
| Dy | - | - | 4.44 | - | - | - | - | - | - | - |
| Ho | 0.88 | 0.9 | 0.71 | 1.26 | 1.13 | 1.20 | 0.96 | 1.26 | 0.78 | 0.87 |
| Er | - | - | 2.2 | - | - | - | - | - | - | - |
| Tm | 0.324 | 0.35 | 0.2 | 0 | 0 | 0.408 | 0.33 | 0.42 | 0.24 | 0.30 |
| Yb | 1.8 | 2.12 | 1.72 | 1.26 | 2.5 | 2.58 | 1.93 | 2.5 | 1.43 | 1.71 |
| Lu | 0.25 | 0.3 | 0.2 | 0.18 | 0.36 | 0.36 | 0.26 | 0.35 | 0.2 | 0.23 |
| Hf | - | 7.99 | 4.3 | - | - | - | 3.92 | 5.27 | 5.09 | 8.56 |

| | | | | | | | | | | |
|---|---|---|---|---|---|---|---|---|---|---|
| Ta | - | 4.26 | 1 | - | - | - | 2.16 | 2.47 | 2.53 | 3.15 |
| W | - | 2.23 | - | - | - | - | 0 | 0.04 | 0.72 | 1.35 |
| Tl | - | - | - | - | - | - | - | - | - | - |
| Pb | - | - | 12.3 | - | - | - | - | - | - | - |
| Bi | - | - | - | - | - | - | - | - | - | - |
| Th | - | 20.1 | 7.7 | - | - | - | 4.95 | 10.1 | 9.14 | 9.91 |
| U | - | 5.48 | 2.5 | - | - | - | 1.83 | 3.51 | 2.93 | 3.26 |

**Isotopic Data**

Also for bulk rock chemistry, samples were also analyzed for isotopic composition of strontium. Samples included into the isotopic portion of this study include: two radial dikes, two cognate xenoliths, and two miarolitic cavities. Of the samples included, isotopic work has never before been conducted on miarolitic cavities within the Spanish Peaks intrusive suite, so this work reveals important information about the origin of mineral deposits within the cavities. The isotopic data for these samples is found in Table 4.7.

Samples from other studies, (Penn (1994), and Miggins (2002)) are included in this study to compare against strontium isotope values of radial dikes analyzed in this study, as well as to gain an understanding of what the strontium isotopic values of the West Spanish Peak stock are. Isotopic data from these other studies can be found in Table 4.8.

**Table 4.7:** Strontium isotopic data for samples analyzed in this study, Rb and Sr values reported in parts per million (ppm).

| **Sample** | **SR-7** | **IC-SPD4** | **IC-7** | **IC-14a** | **TJ-2E** | **TJ-3B** |
|---|---|---|---|---|---|---|
| Type | Radial Dikes | | Cognate Xenoliths | | Miarolitic Cavities | |
| Rb (ppm) | 29.73 | 30.99 | 4.60 | 1.00 | 12.81 | 18.48 |
| Sr (ppm) | 1098 | 1059 | 1288 | 371.6 | 980.9 | 2366 |

| | | | | | | |
|---|---|---|---|---|---|---|
| $(^{87}Sr/^{86}Sr)_m$ | 0.715952 | 0.706717 | 0.704993 | 0.706411 | 0.710312 | 0.718595 |
| Uncertainty (2σ) | ± 0.000008 | ± 0.000009 | ± 0.000009 | ± 0.000007 | ± 0.000010 | ± 0.000009 |

**Table 4.8:** Strontium isotopic data for samples from other studies in the Spanish Peaks Region, Rb and Sr values reported in parts per million (ppm).

| **Sample** | **sp33** | **98-48** | **sp73** | **sp95** | **sp101** |
|---|---|---|---|---|---|
| Type | WSP Stock | | Radial Dikes | | |
| Source | Penn (1994) | Miggins (2002) | Penn (1994) | Penn (1994) | Penn (1994) |
| Rb (ppm) | 38.10 | 79.40 | 87.2 | 49.8 | 50.7 |
| Sr (ppm) | 738.3 | 303.0 | 735.0 | 1107 | 847.4 |
| $(^{87}Sr/^{86}Sr)_m$ | 0.704200 | 0.704153 | 0.707366 | 0.706077 | 0.704823 |
| Uncertainty (2σ) | ± 0.000013 | ± 0.000018 | ± 0.000014 | ± 0.000012 | ± 0.000013 |

# Chapter 5

## *Discussion and Conclusions*

### Introduction

By understanding the geochemical constraints necessary to generate the intrusive features in the Spanish Peaks region, a more comprehensive understanding of the origin of this igneous complex can be revealed. The data collected for this project in conjunction with the synthesis of data collected from recent studies by Penn (1994), Miggins (2002), Contreras (2014) and Johnson (2014), portrays magmatism in the Spanish Peaks area in a new light. There is an indication based on the timing of events and the major element chemistry of igneous features that the West Spanish Peak and the radial dikes around the peak share a common magma source. This magma body was fed by melts from a rising asthenosphere that was associated with the opening of the Rio Grande Rift approximately 25 Ma. By understanding the chemical nature of features included within the radial dike swarm, specifcally cognate xenoliths and miarolitic cavities, it is possible to obtain a better picture of how these features originated, became included into the matrix of these radial dikes, and influenced their petrogenesis.

The timing of intrusion of igneous features has been the focus of previous studies, namely Penn (1994) and Miggins (2002), and these two geochronologic studies both suggest that the timing of intrusion of the West Spanish Peak and the radial dike swarm overlap one another. The overlap of

intrusive ages of these igneous features suggest that a common magma source is, at the least, possible for these features. The timing of intrusive events is one of the major assumptions made in this study since no new geochronologic work was performed to determine the age of specific features. In the context of this study, it means that the ages of cognate xenoliths included into the radial dikes are assumed to have an approximately contemporaneous ages as the emplacement of the radial dikes themselves.

The discovery of cognate xenoliths and miarolitic cavities contained within the radial dikes around West Spanish Peak, first described by Contreras (2014) and Johnson (2014) respectively, was an indication that the chemical nature of the radial dikes around West Spanish Peak has not been fully explored because no indication of these features has been reported in previous studies. Based on the major element chemistry analyses in this study, as well as mineral and trace element chemistry studies conducted by Contreras (2014), the cognate xenoliths appear to show a very regular pattern of chemical variation chemical relationship with the radial dikes as well as the West Spanish Peak stock, indicating that these features very possibly share a common, parent magma. On the other hand, based on isotopic data performed in this study the miarolitic cavities within the radial dikes appear to be unrelated to other intrusive features in the West Spanish Peak intrusive suite, thus indicating that the miarolitic cavities did not form in a purely magmatic environment like other features in the area, but rather were deposited by groundwater passing through the upper crust after the intrusion of the radial dikes which these features are found within.

### Isotopic $^{87}Sr/^{86}Sr$ Implications for the Spanish Peaks Region:

The measured $^{87}Sr/^{86}Sr$ values for newly analyzed samples and from previous studies are synthesized (Fig. 5.1) in order to obtain a better history of the strontium isotopic evolution of the area. $^{87}Sr/^{86}Sr$ values for the West Spanish Peak stock are relatively low, ranging only from 0.704153 to 0.704200. $^{87}Sr/^{86}Sr$ values for the radial dikes on the other hand vary from 0.704823 to 0.715952, suggesting that there has been significant groundwater interaction, mobilizing metals such as strontium, but this has not affected all the dikes to the same degree because values of < 0.710000, ranging from 0.704823 to 0.707366, are still reported for four out of the five radial dikes compared. $^{87}Sr/^{86}Sr$ values for the cognate xenoliths are more similar to the values reported for the West Spanish Peak stock and radial dikes, ranging from 0.704993 – 0.706411.

The reported $^{87}Sr/^{86}Sr$ values for the miarolitic cavities are exceptionally high, ranging from 0.710312 to 0.718595, indicating that their presence is closely associated with groundwater interaction not magmatic fluids associated with the radial dikes they are found within. The high values, > 0.710000, imply that the presence of many mineral phases contained within these cavities are likely to have precipitated out of groundwater solution that equilibrated with older Proterozoic basement rocks in the area. The concentration of oxides and sulfides, especially the cobalt sulfide carrollite found in sample TJ-2a, indicates that metals were dissolved by these groundwaters and they may have been hot, possibly heated by the intrusion of the West Spanish Peak stock.

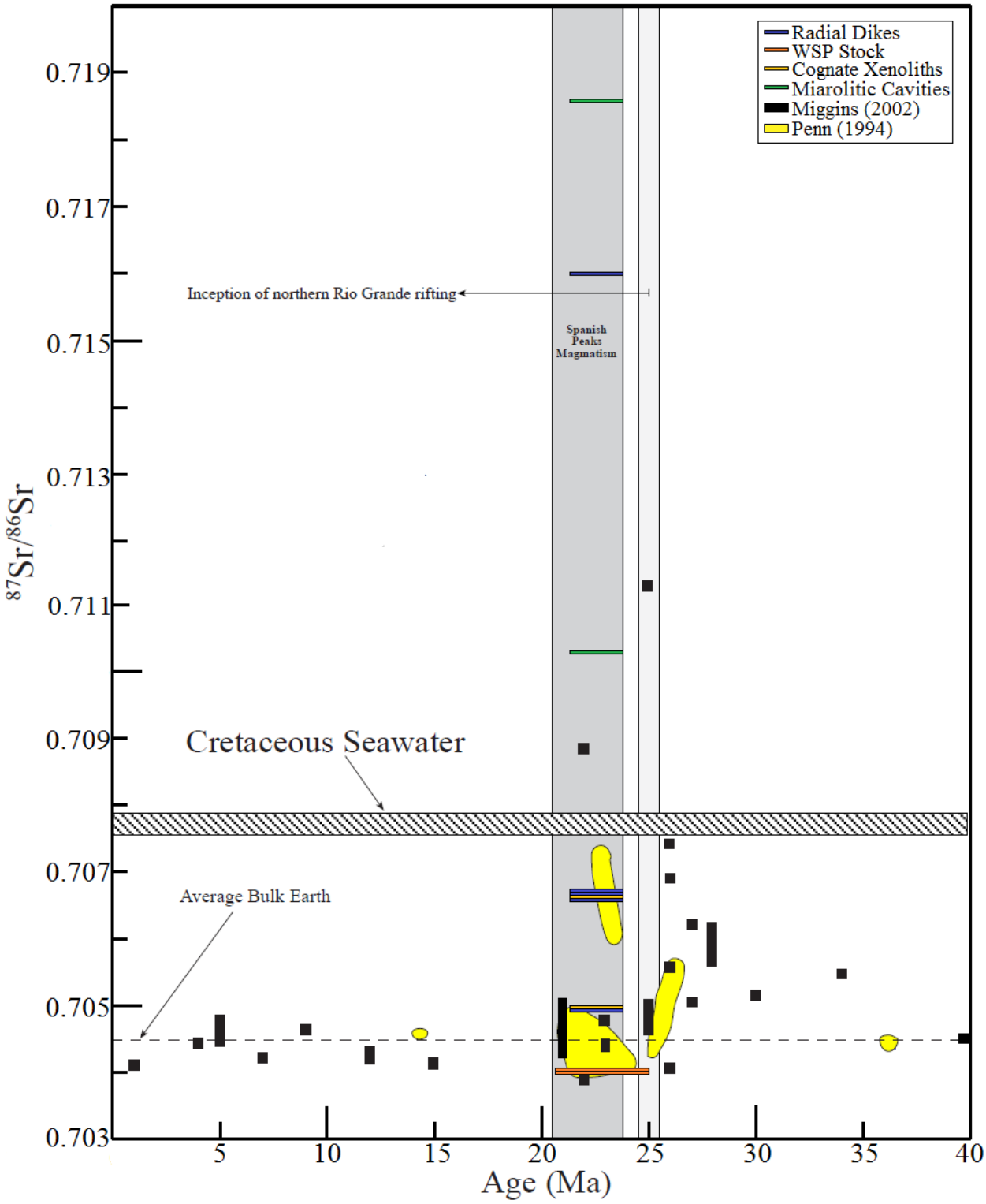


**Figure 5.1:** A modified figure taken from Miggins (2002) plotting age versus the measured ($^{87}Sr/^{86}Sr$) values of various intrusive features included in this study as well as ($^{87}Sr/^{86}Sr$) values from Penn (1994) & Miggins (2002) respectively. Notice high ($^{87}Sr/^{86}Sr$) values for miarolitic cavities, and a radial dike which hosted miarolitic cavities, indicating groundwater interaction.

***Cognate Xenoliths, Radial Dikes, and the West Spanish Peak Stock***

While all the intrusive features found in the Spanish Peaks region do not share the exact same isotopic $^{87}Sr/^{86}Sr$ values, the West Spanish Peak Stock, the radial dikes, and the cognate xenoliths incorporated into these dikes do display $^{87}Sr/^{86}Sr$ values that fall well within the range of all other igneous features in the area reported by Penn (1994) and Miggins (2002). It is clear there is not an absolute isotopic equilibrium for these features, however it is possible some degree of alteration has occurred, leading towards the comparatively high $^{87}Sr/^{86}Sr$ levels of the miarolitic cavities found within the same region. However, the fact that West Spanish Peak Stock, the radial dikes, and the cogmate xenoliths $^{87}Sr/^{86}Sr$ values are within the same range found for other igneous rocks in the West Spanish Peaks region indicates that a common parent magma is not out of the question. There could have possibly been differing degrees of assimilation of country rock between these three igneous features, effectively contaminating upwelling magmas with additional strontium from surrounding material that the magmas rose through. As a result, the low $^{87}Sr/^{86}Sr$ values associated with magmas fed by an upwelling asthenosphere would rise as varying degrees of country rock were assimilated to form the stock, radial dikes and xenoliths.

***Miarolitic Cavities***

One of the major conclusions drawn from this study is that the origin of miarolitic cavities found within the radial dikes around West Spanish Peak are not associated with magmatic waters relaeased by the intrusion of igneous features of the region as a whole. This was determined by the isotopic analysis of $^{87}Sr/^{86}Sr$ values of the two miarolitic cavities analyzed in this study, yielding 0.710312 and 0.718595 respectively. The high values reported were not expected based on the work done by Johnson (2014), who based on petrographic and trace element analyses of a suite of miarolitic cavites suggested that these features exsolved from the dike-forming magma. However, based on the reported istopoic values of $^{87}Sr/^{86}Sr$, it can be concluded that the miarolitic cavites in fact were precipitated from a non-intrusive fluid, likely groundwater, that flowed throughout the dikes mobilizing materials that then formed within the available cavity space as groundwater flowed out of the region. Part of the implications of this model are that the dikes must have already intruded and been formed for these mineral phases to become deposited within them, indicating that this paleo-groundwater event, or events, occurred after the emplacement of the radial dike swarm.

The mobilization of elements within groundwater fluid that mineralized these cavities is

reflected by the composition of the minerals present within the cavities. Quartz, epidote, chlorite, muscovite, calcite, hematite, pyrite, chalcopyrite, barite, and carollite are all minerals found within the miarolitic cavities and from this it can be determined that Si, Al, Fe, Mg, Ca, S, Cu, Ba, and Co were all elements that were mobilized by this fluid. In fact, one of the dikes within which these miarolitic cavities were found also displayed an arbitrarily high $^{87}Sr/^{86}Sr$ value of 0.715952, indicating that the groundwater fluid which deposited minerals into available cavities also flowed through the dike, equilibrating the strontium levels with the surrounding country rocks. As a result, the altered strontium isotopic values of the host dikes appear to be higher than that of other intrusive features in the West Spanish Peak area.

**Cogenetic Model for West Spanish Peak, Radial Dikes, and Cognate Xenoliths:**

Based on the bulk oxide comparisons demonstrated in the Harker diagrams (Fig 4.1), as well as based on similar comparison diagrams for trace elements done by Contreras (2014), it appears that there is a genetic relationship between the igneous features found in the Spanish Peaks intrusive complex. The samples included into the Harker variation diagrams are a conglomerate of samples collected for this study as well as from Penn (1994), and Miggins, (2002).

There appears to be a mixing line from which can be derived the composition of the West Spanish Peak stock, radial dikes, cognate xenoliths as well as intrusive sills, in the majority of Harker variation diagrams, but this relationship is strongest in between FeO, MgO, CaO, $K_2O$, and TiO in regards to $SiO_2$. The cognate xenoliths represent the most mafic crystallization products of these intrusives, high in regard to iron and magnesium with low silica and potassium, while the West Spanish Peak stock generally represents the more felsic, low iron, calcium, and magnesium with high silica and potassium. The radial dikes and intrusive sills show intermediate levels, but form a linear relationship between the mafic cognate xenoliths and the felsic West Spanish Peak stock. In fact, there are a few radial dikes that show slightly more felsic compositions than the West Spanish Peak stock, but they too exist along these mixing lines.

It is important to note that variation exists between the two cognate xenolith samples included in this study because these two samples were cognate xenoliths representing end member groups of xenolith composition, as described by Contreras (2014). One end member group is the cognate xenoliths which were composed of primarily plagioclase feldspar and amphibole, such as Sample IC-7 included in this study. The other end member xenolith group is the cognate xenoliths composed of

predominantly clinopyroxne and amphibole, such as sample IC-14a included in this study. There was a third group showing intermediate variations between plagioclase feldspar, clinopyroxene, and amphibole, but of this group there was in general more plagioclase feldspar and amphibole than clinopyroxene. It is also important to note that Sample IC-14a was the only sample described by Contreras (2014) to display abundant clinopyroxene with a distinct absence of plagioclase feldspar, while there was a higher amount of plagioclase-amphibole rich end member samples. The indication from this is that the plagioclase-amphibole rich cognate xenoliths are more compatible, and are thus not only more common, but are more important the role of mixing of compositions from which the other intrusive features can be derived from.

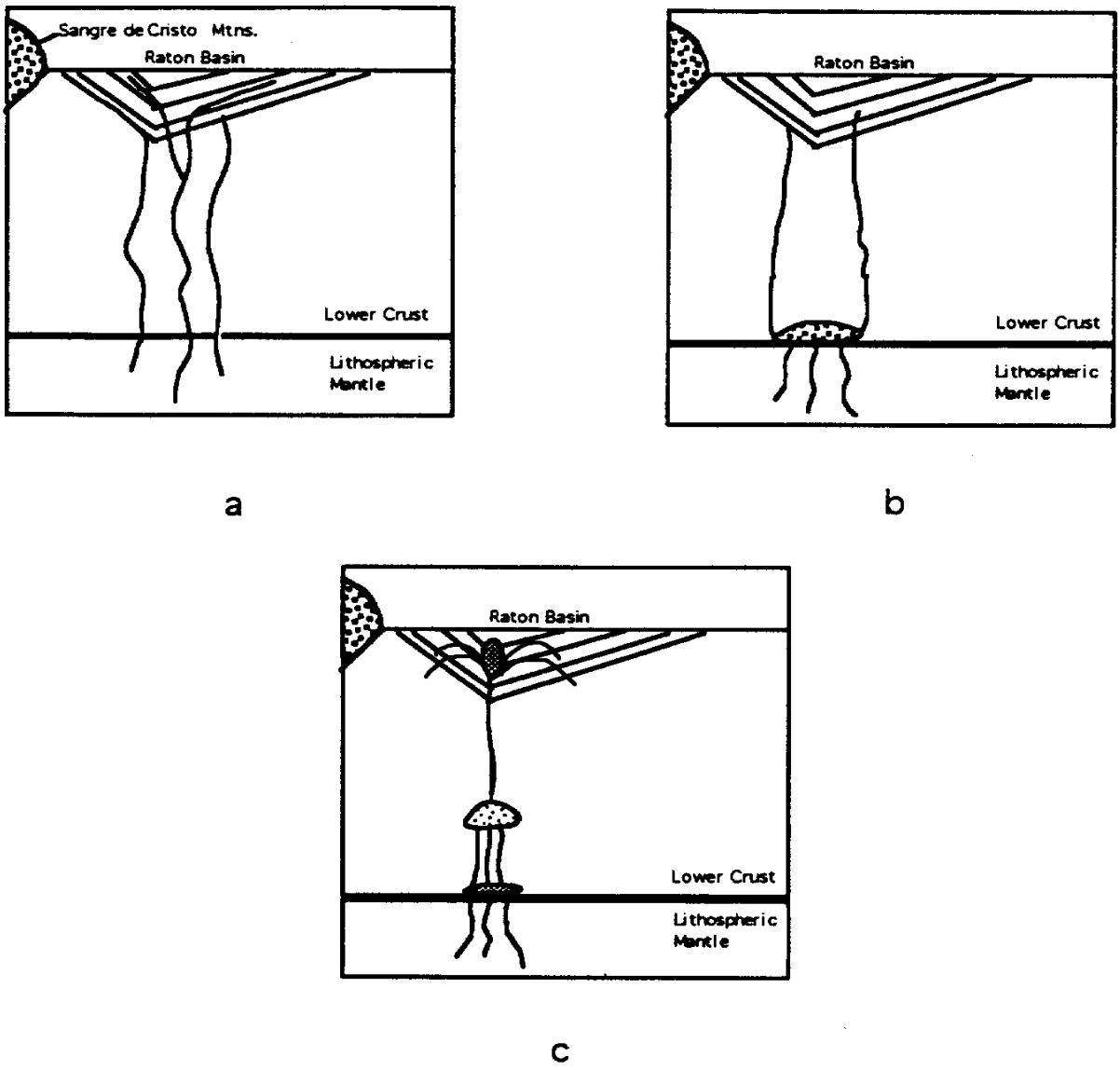


**Figure 5.2 (a), (b), (c):** A modified figure taken from Penn (1994), displaying snapshots of the regional intrusive history of the Raton Basin. 5.2(a): Emplacement of mafic dikes and sills at beginning of Spanish Peaks magmatic period; approximately 25 Ma. 5.2(b): Common, parent magma body forms at crust-mantle lithosphere boundary; approximately 25 Ma. 5.2(c): Emplacement of the West Spanish Peak stock, formation of a secondary magma body within the crust from which cognate xenoliths formed in, as well as the intrusion of radial dikes around West Spanish Peak, all fed by parent-magma body; approximately 21-25 Ma.

The above petrographic model (Fig. 5.2), modified from Penn (1994), can the be used to generalize the formation of igneous features found within the Spanish Peaks intrusive suite. The formation of intrusive features at all in this region due to the rising asthenosphere and the opening of

the Rio Grande Rift, to the west of the Sangre de Cristo Mountians in the snapshots depicted. Melting associated with decompression of overlying material due to the thinning of the crust climbed up the margin of the Rio Grande Rift into an area of thrust faulting associated with the formation of the Sangre de Cristo mountains during the Laramide Orogeny. (Fig. 5.2(a)) is a representation of this, showing how the partial melting of hydrous magmas formed the first mafic dikes and sills intruding into the Raton Basin. (Fig. 5.2(b)) then shows how the pooling of magma at the crust mantle lithosphere boundary as the lower crust begins to undergo a partial melt. The inflow of more mafic magmas associated with the opening of the Rio Grande Rift would cause a lateral expansion of a concentrated silicic body, while mafic magmas would still be able to climb around the margin of this magma body. Huerfano's Butte is an example of mafic material that likely climbed up the margin of such a magma body, and there are other mafic features which form around the periphery of the primarily more silicic magmas that formed the Spanish Peaks and the radial dikes. This laterally spreading magma pool at the crust lithospheric mantle boundary was the most likely parent magma body from which all the observable features in this study are derived from.

(Fig. 5.2(c)) the represents the intrusion of the West Spanish Peak plutonic stock into the Raton Basin, fed by the common parent magma, which overlaps with the time window for the intrusion of the radial dike swarm around the mountain. The formation of cognate xenoliths was discussed in a similar model by Contreras (2014), which suggests that there was a secondary magma chamber, fed by the parent magma chamber, in which the crystallization of large phenocrysts displayed in the cognate xenoliths could take place while this chamber cooled slowly. It is in this secondary magma chamber in the crust in which mafic minerals would begin to fractionally crystalize out of the magma, namely amphibole, plagioclase, and clinopyroxene, forming the composition of the cognate xenoliths. However simultaneously while this secondary chamber cools, radial dikes are being fed by the parent magma body below up the plumbing system through which the West Spanish Peak stock intruded. In certain cases, these rising radial dikes would cross the secondary magma chamber on their rise to the surface, incorporating these cognate xenoliths into the matrix of the radial dikes. It is after all of the displayed snapshots that East Spanish Peak intrude, and the subsequent weathering of sediments of the Raton Basin have exposed these igneous features to the surface as they are seen today.

**Future Work:**

To further investigate whether the radial dikes around West Spanish Peak share a co-genetic relationship with the West Spanish Peak plutonic stock, a larger regional investigation of temporal and geochemical relationships can be performed on radial dikes to see if a co-genetic relationship exists for them as well. Specifically, more geochemical work on very large, well known, regional radial dikes such as the "Great Wall" dike and the "Devil's Staircase" dike could be performed. If samples were collected from these dikes as well as a few other dikes that appear to contact the plutonic stock, ultimately providing data over a larger geographic area within the West Spanish Peaks region. It can then be determined if characteristics and included features in this study are localized phenomena or if they affected the radial dike swarm as a whole. The reason any future investigation may prove fruitful to a more regional geochemical relationship is that samples from this study, as well as samples from Contreras (2014) and Johnson (2014), were all collected from a concentrated area on the southwestern limb of the West Spanish Peak, potentially limiting the scope to which the implications of this study can apply to the Spanish Peaks intrusive suite as a whole.

**Acknowledgments:**

To begin, I would like to thank the University of Colorado and the Department of Geological Sciences for guiding me throughout my undergraduate career, and for granting me the mental tools necessary to complete this project. I would also like to thank Charles Stern for his tremendous help in guiding me during throughout entirety of this project, without him this project would absolutely not be possible. The University Research Opportunity Program and Mentorship Program also deserves recognition for providing funding for the analyses necessary to complete this honors thesis. In addition, a thank you to Lang Farmer and Emily Verplanck for allowing me to prepare samples in their isotope lab as well as running strontium isotopes in their mass spectrometer, and ACTLABS in Canada for operating the ICP-MS necessary to obtain major weight percent oxides, trace element, and rare-earth element. I would also like to thank Julian Allaz for allowing Charles Stern and I the use of the Electron Microprobe, which collected data about chemical composition of individual minerals in this study. I would also like to thank Paul Boni for his countless hours spent guiding me through multiple rounds of making thin sections of rock samples that were included into this study.

## References


Contreras, I. A. R. (2014). *Magmatic evolution and petrochemistry of xenoliths contained within an andesitic dike of western spanish peak, colorado*. Unpublished undergraduate honor's thesis, Geological Sciences, University of Colorado, Boulder.

Johnson, R. B., (1961). Patterns and origin of radial dike swarms associated with west spanish peak and dike mountain, south-central Colorado. *Geological Society of America Bulletin*, *72*, 579–590.

Johnson, R. B., (1968) Geology of the igneous rocks of the Spanish Peaks region Colorado. *U.S. Geological Survey Professional Paper 594*(G), 78.

Johnson, T. A. (2014). *Mineralogy and genesis of miarolitic cavities in altered andesitic dikes on west spanish peak, colorado, usa.* Unpublished undergraduate honor's thesis, Geological Sciences, Univeristy of Colorado, Boulder.

Miggins, D. P. (2002). *Chronologic , geochemical, and isotopic framework of igneous rocks within the raton basin and adjacent rio grande rift, south-central colorado and northern new mexico*. Unpublished master's thesis, University of Colorado at Boulder.

Penn, B.S. (1994). *An investigation of the temporal and geochemical characteristics, and the petrogenetic origins of the spanish peaks intrusive rocks of south-central colorado.* Published doctoral dissertation, Colorado School of Mines.

Penn, B. S., & Lindsey, D. A. (2009). $^{40}Ar/^{39}Ar$ dates for the spanish peaks intrusions in south-central colorado. *Rocky Mountain Geology*, *44*(1), 17-32.

Smith, R. P., (1975). *Structure and petrology of spanish peaks dikes, south central colorado.* Published doctoral dissertation, University of Colorado at Boulder.

Stormer, J. C., Jr., (1972). Ages and nature of volcanic activity on the southern high plains, new mexico and colorado: *Geological Society of America Bulletin, 83*, 2443–2448.